NASA CR54639

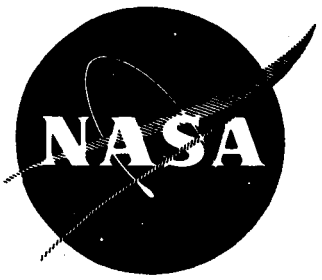

STEADY-STATE CREEP OF DISPERSION-STRENGTHENED METALS

by

B. A. Wilcox and A. H. Clauer

prepared for

NATIONAL AERONAUTICS AND SPACE ADMINISTRATION

CONTRACT NAS 3-7615

BATTELLE
MEMORIAL INSTITUTE

NOTICE

This report was prepared as an account of Government sponsored work. Neither the United States, nor the National Aeronautics and Space Administration (NASA), nor any person acting on behalf of NASA:

A.) Makes any warranty or representation, expressed or implied, with respect to the accuracy, completeness, or usefulness of the information contained in this report, or that the use of any information, apparatus, method, or process disclosed in this report may not infringe privately owned rights; or

B.) Assumes any liabilities with respect to the use of, or for damages resulting from the use of any information, apparatus, method or process disclosed in this report.

As used above, "person acting on behalf of NASA" includes any employee or contractor of NASA, or employee of such contractor, to the extent that such employee or contractor of NASA, or employee of such contractor prepares, disseminates, or provides access to, any information pursuant to his employment or contract with NASA, or his employment with such contractor.

FINAL REPORT

STEADY-STATE CREEP OF DISPERSION-STRENGTHENED METALS

by

B. A. Wilcox and A. H. Clauer

prepared for

NATIONAL AERONAUTICS AND SPACE ADMINISTRATION

August 19, 1966

CONTRACT NAS 3-7615

Technical Management
NASA Lewis Research Center
Cleveland, Ohio
F. H. Harf
W. S. Cremens

BATTELLE MEMORIAL INSTITUTE
Columbus Laboratories
505 King Avenue
Columbus, Ohio 43201

STEADY-STATE CREEP OF DISPERSION-STRENGTHENED METALS

by

B. A. Wilcox and A. H. Clauer

ABSTRACT

The high-temperature creep behavior of "recrystallized" Ni-ThO_2 alloys has been studied using vacuum constant-stress creep conditions. Five alloys, containing different volume fractions of ThO_2 and different ThO_2 particle-size ranges were creep tested at various stresses (nominally 2,000-15,000 psi) and temperatures (nominally 600-1050°C).

Emphasis has been placed on rationalizing the mechanical behavior in terms of the structural changes occurring during creep deformation. Mechanical and structural studies indicated that the rate-controlling creep process was the climb of edge dislocations over ThO_2 particles. A modified version of the Ansell-Weertman climb theory has been developed. The theory relates the steady-state creep rate to stress, temperature, and the ThO_2 particle size and spacing.

LIST OF SYMBOLS

$\dot{\epsilon}_s$ = steady-state creep rate

α = fractional volume of deformable matrix

σ = true stress (applied)

σ_e = effective stress

σ_i = internal stress

b = Burgers vector

D = coefficient of self-diffusion in the matrix = $D_o \exp - (Q_{s.d.}/RT)$

k = Boltzmann's constant

R = gas constant

T = absolute temperature

T_m = absolute melting temperature

f = volume fraction of dispersed phase

$2r_v$ = average particle diameter (for spherical particles)

$2r_s$ = average planar particle diameter

d = mean planar center-to-center particle spacing

λ = mean free path between particles

μ = shear modulus

n = the number of dislocations piled up against particles

m = stress exponent

$B, \beta, C, K, K', K'', \rho_o, D_o$ = constants

Q_c = apparent activation energy for creep

$Q_{s.d.}$ = activation energy for self-diffusion in matrix

ρ_T = total dislocation density

L = the total length of a set of random lines drawn on a micrograph

N' = number of intersections which dislocations make with the set of grid lines

t = thickness of thin foils

M = plate or print magnification

τ_p = Orowan bowing stress

ϕ = averaging factor for the screw-edge character of a bowed-out dislocation loop

N = number of points per unit volume where climb of dislocations over particles can occur

A = area swept out per climb event

R = climb rate

ρ_{em} = density of mobile edge dislocations

$\bar{x}$ = distance between effective pinning points along a dislocation

TABLE OF CONTENTS

APPENDIX

LIST OF TABLES

LIST OF FIGURES

LIST OF FIGURES
(Continued)

STEADY-STATE CREEP OF DISPERSION-STRENGTHENED METALS

by

B. A. Wilcox and A. H. Clauer

SUMMARY

The following Ni-ThO_2 alloys, prepared by Sherritt Gordon Mines, Ltd., were creep tested at temperatures greater than 0.5 T_m.

Alloy	Average ThO_2 Particle Diameter $2r_v$, Å	Mean Planar Center-to-Center Particle Spacing d, Å
(A) Ni + 1.00 vol % ThO_2	220	2505
(B) Ni + 2.56 vol % ThO_2	219	1760
(C) Ni + 1.00 vol % ThO_2	428	5290
(D) Ni + 2.66 vol % ThO_2	526	3670
(E) Ni + 4.41 vol % ThO_2	549	2990

It was found for each alloy that the steady-state creep rate, $\dot{\epsilon}_s$, could be expressed empirically by

$$\dot{\epsilon}_s = \frac{C}{T}\sigma^m \exp -\left(\frac{Q_c}{RT}\right) \quad ,$$

where C is a constant for a given alloy, T is absolute temperature, and σ is the applied stress. The stress exponent m was ~7 and the activation energy for creep, Q_c, was 64 kcal/mole, which agrees closely with the activation energy for self-diffusion in nickel ($Q_{s.d.}$ Ni = 61-67 kcal/mole).

A modified version of the Ansell-Weertman dislocation climb theory was developed and applied to the experimental creep results. The theory predicts that the creep rate of these alloys is related to the particle size and spacing by

$$\dot{\epsilon}_s \propto d^3/r_v\lambda \quad ,$$

where λ is the mean free path. Comparison of the creep rates of several alloys at constant stress, temperature, and initial microstructure showed that this relation was obeyed.

INTRODUCTION

The many theories proposed to explain the influence of dispersed second-phase particles on the yield strength and flow stress of metals have been reviewed by Kelly and

Nicholson[1]* and Ansell[2]. Until recently, only a few attempts[3-5] had been made to develop mechanistic treatments that characterize the creep behavior of dispersion-strengthened metals, and to date these have not been fully evaluated experimentally. Weertman[3] and Ansell and Weertman[4] proposed a quantitative creep theory for coarse-grained dispersion-strengthened metals, based on the concept that the rate-controlling process for steady-state creep was the climb of dislocations over second-phase particles, as suggested by Schoeck[6]. The theory predicted that the steady-state creep rate, $\dot{\epsilon}_s$, was proportional to the applied stress, σ, for low stresses and that $\dot{\epsilon}_s \propto \sigma^4$ for high stresses. Ansell[2] has extended the low-stress model to include the case where pile-ups are present and this aids the climb of the lead dislocation over a particle. This variation of the climb model gives $\dot{\epsilon}_s \propto \sigma^2$. The activation energy for creep, Q_c, was equivalent to that for self-diffusion, $Q_{s.d.}$, in the matrix. Some limited experimental evidence in support of this theory was obtained on a recrystallized Al-Al_2O_3 SAP-type alloy by Ansell and Lenel.[7]

Ansell and Weertman[4] also developed a semiquantitative theory for high-temperature creep of fine-grained dispersion-strengthened metals in order to explain their results on an extruded SAP-type alloy, which had a fine-grained fibrous structure. They suggested that the rate of dislocation generation from grain boundaries was the rate-controlling process and fitted their results to the equation

$$\dot{\epsilon}_s = K \exp -\left(\frac{Q_c - K' \sigma}{kT}\right) , \qquad (1)$$

where Q_c was found to be 150 kcal/mole, i.e., $Q_c \approx 4\, Q_{s.d.}$ in aluminum. More recently Wilcox and Clauer[8] examined the steady-state creep of TD Nickel bar (Ni + 2 vol % ThO_2) over the temperature range 325-1100°C and the stress range 15,000-36,000 psi. At high temperatures (above 0.5 T_m) it was found that grain-boundary sliding was the most important mode of creep deformation, and the steady-state creep rate, $\dot{\epsilon}_s$, was related to stress and temperature by an empirical equation of the form

$$\dot{\epsilon}_s = K'' \sigma^m \exp -\left(\frac{Q_c}{RT}\right) , \qquad (2)$$

where Q_c = 190 kcal/mole and m had an unusually high value of 40. A creep mechanism based on cross slip of dislocations around ThO_2 particles satisfactorily explained the low-temperature ($T < 0.5\ T_m$) creep behavior of TD Nickel, and the following relation was applicable:

$$\dot{\epsilon}_s = B \exp -\left(\frac{Q_c(\sigma)}{RT}\right) . \qquad (3)$$

$Q_c(\sigma)$ was found to decrease from 57 to 46 kcal/mole as the stress was increased from 32,000 to 36,000 psi.

The theoretical and empirical relations that have been used to describe the creep behavior of dispersion-strengthened metals are summarized in Table 1.

Although there is no general agreement regarding the mechanisms involved in the creep of dispersion-strengthened metals, it has become apparent that second-phase particles can affect the creep strength of metals in two ways[10]:

*References are given on page 35.

TABLE 1. PREVIOUSLY REPORTED STEADY-STATE-CREEP RELATIONSHIPS FOR DISPERSION-STRENGTHENED METALS

Condition		Creep Equation	Applicable Examples	Reference
Coarse-grained materials, low stresses	(A)	$\dot{\epsilon}_s = \frac{\alpha\pi\sigma b^3 D}{2kT(2r_v)^2}$	Possibly recrystallized SAP	(3, 4)
Coarse-grained materials, high stresses	(B)	$\dot{\epsilon}_s = \frac{\alpha 2\pi\sigma^4 d^2 D}{(2r_v)\mu^3 kT}$, for $\frac{n\sigma b^3}{kT} < 1$	Possibly recrystallized SAP	(3, 4, 7)
Coarse-grained materials, high stresses	(C)	$\dot{\epsilon}_s = \frac{\alpha\pi\sigma^2 dD}{\mu^2 b^2 (2r_v)} \exp\left(\frac{2\sigma^2 db^2}{\mu kT}\right)$, for $\frac{n\sigma b^3}{kT} > 1$	Possibly recrystallized SAP	(3, 4)
Fine-grained materials (grain size $\lesssim 5\ \mu$)	(D)	$\dot{\epsilon}_s = K \exp -\left(\frac{Q_c - K'\sigma}{kT}\right)$	Extruded SAP	(4)
Materials with stable, fine, fibrous grain structure	(E)	$\dot{\epsilon}_s = K''\sigma^m \exp -\left(\frac{Q_c}{RT}\right)$, for $T > 0.5\ T_m$	TD Nickel bar	(8)
Materials with stable, fine, fibrous grain structure	(F)	$\dot{\epsilon}_s = B \exp -\left(\frac{Q_c(\sigma)}{RT}\right)$, for $T < 0.5\ T_m$	TD Nickel bar	(8)

Definitions of symbols are listed at front of report.

(1) By particles acting as barriers to moving dislocations during creep

(2) By the influence that particles have on the development of the structure during fabrication (e.g., grain size, substructure), and the subsequent effect of the structure on dislocation mobility during creep.

Thus the distinction that Ansell[2] has made between "direct dislocation-particle interactions" and "indirect dislocation-particle effects" with regard to yield strength, applies to creep strength as well. The authors have recently compared the high temperature creep behavior of TD Nickel [an example of Case (2)] with that of several recrystallized Ni-ThO_2 alloys* [example of Case (1)][10].

At the start of this investigation, it was felt that the lack of general agreement concerning creep mechanisms was due in part to the absence of detailed studies relating the structures of crept specimens to the mechanical behavior. Thus the present work on thoriated nickel alloys was undertaken with the aim of studying the structural changes that occur during creep of dispersion-strengthened metals and of rationalizing the observed mechanical behavior in terms of the creep structures.

EXPERIMENTAL METHODS

Creep testing was done in a vacuum of 10^{-5} torr under constant (tensile) stress conditions using a lever arm similar to that described by Fullman, et al.[11] The specimen design is shown in Figure 1, and gripping was accomplished by both pin-loading and clamping with split serrated grips made from TD Nickel bar. Creep extension was measured with a sensitivity of 50-100 microinches by two sliding molybdenum extensometers scribed with fiducial marks, one on each side of the specimen gage length.

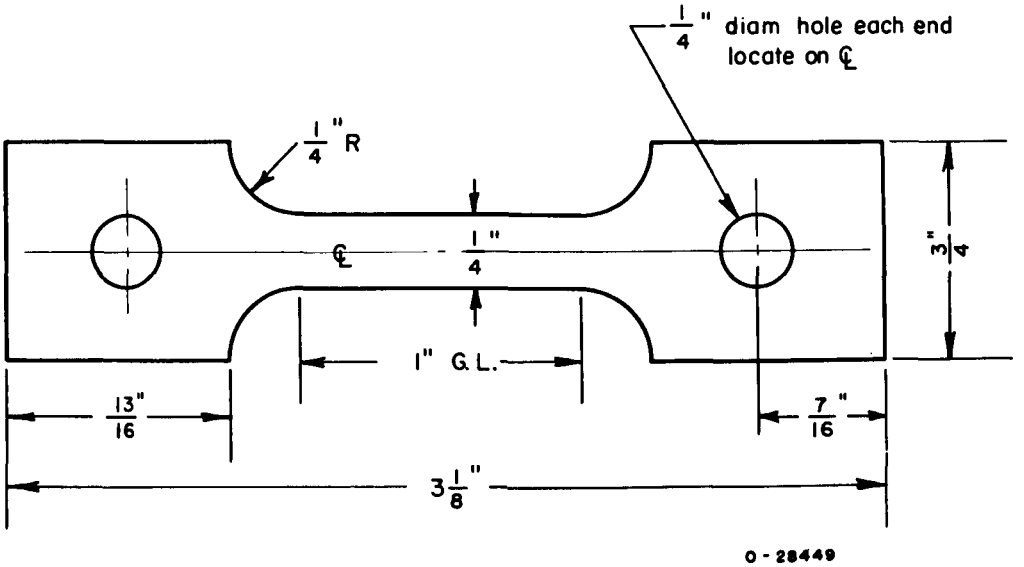

FIGURE 1. DESIGN FOR 20-MIL SHEET CREEP SPECIMENS

*The recrystallized Ni-ThO_2 alloys discussed in Reference (10) are Alloys A, B, and C, which are described in this report.

The jet indentation technique was used for preparing thin foils of as-received and crept specimens for transmission electron microscopy. Final thinning was done in a solution of 20 percent perchloric acid-80 percent ethyl alcohol, and electron microscopic examination was accomplished with a Siemens Elmiskop IA. The fractographic and metallographic replication techniques used in this work have been described elsewhere[8,9].

MATERIALS

In order to study the effects of ThO_2 particle size and volume fraction on the elevated-temperature creep behavior of Ni-ThO_2 alloys, five compositions in the form of 20-mil sheet were obtained from Sherritt Gordon Mines Ltd., Fort Saskatchewan, Alberta, Canada (see Table 2). Chemical analyses of all five alloys showed there was very little variation of trace elements from one material to another (Table 3).

Material Fabrication

Since it was desired that the materials have recrystallized structures, Sherritt Gordon employed a fabrication technique different from that used to produce their optimum DS Nickel sheet.[12] The method was intended to produce alloys having similar grain sizes and substructures, with a minimum of mechanical anisotropy in the final sheets. The fabrication of these experimental alloys may be summarized as follows:

(1) Isostatic compacts were prepared using 30,000 psi compacting pressure. The compacts were trimmed to measure 1-1/2 x 4 x 0.20 inch.

(2) The compacts were sintered at 1200°C for 2 hours in pure, dry hydrogen.

(3) The sintered compacts were preheated in hydrogen to 1090°C and directly hot rolled. The hot reduction was 30 percent, and the hot-rolling direction was perpendicular to the major axis of the compact. This hot-rolling procedure was repeated and, after the second hot reduction, all compacts were 0.090 inch thick.

(4) The hot-rolled pieces were annealed at 1200°C for 1/2 hour and then given a 10 percent thickness reduction in the same direction as the hot-rolling reduction. After cold rolling, the pieces were annealed (1200°C for 1/2 hour) and given a second cold-rolling reduction (10 percent) at right angles to the direction of first cold reduction. This cold roll – anneal cycle was repeated until the strips were 0.020 inch thick, i.e., the rolling direction was rotated 90° for each cycle.

This technique, employing cross-rolling, resulted in materials that had relatively little mechanical anisotropy, i.e., the tensile strength at 870°C did not vary greatly for specimens that were machined with their axes parallel to both directions of the sheet (see Table 2).

TABLE 2. EXPERIMENTAL Ni-ThO_2 ALLOYS

Alloy	Analyzed wt % ThO_2	Calculated vol % ThO_2	Nominal Range of Particle Diameters, Å	Average Particle Diameter, $2r_v$, Å	Average Planar Particle Diameter[a] $2r_s$, Å	Mean Planar Center-to-Center Particle Spacing d, Å	Ultimate Tensile Strength at 870 C, psi[b]
A	1.12	1.00	75-695	220	180	2505	16,400;16,300
B	2.88	2.56	75-835	219	179	1760	23,800;20,800
C	1.12	1.00	150-1390	428	350	5290	16,400;15,900
D	3.00	2.66	150-1500	526	429	3670	18,700;17,800
E	4.97	4.41	150-1500	549	447	2990	18,900;16,000

(a) The planar particle diameter is given by $2r_s = 2r_v\sqrt{2/3}$.

(b) Tests were performed by Sherritt Gordon, in both directions of the sheets.

TABLE 3. CHEMICAL ANALYSIS OF EXPERIMENTAL ALLOYS FOR TRACE ELEMENTS[a]

Element	Weight Percent				
	Alloy A	Alloy B	Alloy C	Alloy D	Alloy E
P	<0.003	0.006	0.003	0.006	0.003
S	0.002	0.011	0.009	<0.002	<0.002
Si	0.003	0.005	0.005	0.003	0.003
Fe	0.02	0.03	0.03	0.02	0.02
Mg	<0.003	<0.003	<0.003	<0.003	<0.003
Mn	<0.003	<0.004	<0.004	<0.003	<0.003
Co	0.04	0.03	0.03	0.04	0.04
Cu	0.002	0.002	0.002	0.002	0.002
Ti	<0.003	<0.003	<0.003	<0.003	<0.003
Al	0.003	0.003	0.002	0.003	0.003
Cr	0.001	0.005	0.006	0.002	0.003
Ag	<0.001	<0.001	<0.001	<0.001	<0.001
Ca	0.007	0.005	0.005	0.015	0.007
Pb	<0.003	<0.003	<0.003	<0.003	<0.003

(a) P and S were determined by wet chemical analysis, and all other elements by spectroscopy.

Particle-Size Measurements

The particle-size distributions were determined by measuring ~700-900 particles per alloy from transmission electron micrographs using a Zeiss Particle Size Analyzer.[13]* The ThO_2 size distribution for each alloy is plotted in Figure 2, and the average particle sizes are given in Table 2, together with the mean planar center-to-center particle spacing, d. The spacing was calculated from the data in Figure 2 by applying the relation[8]:

$$d^2 = \frac{8}{3\sum_i f_i / r_{v_i}^2} \quad , \tag{4}$$

where f_i = volume fraction of particles of a given size having an average particle radius, r_{v_i}.

Structures of the Uncrept (As-Received) Alloys

Since this investigation emphasizes the structural aspects of creep (i.e., rationalization of the mechanical behavior in terms of the observed creep structures), a careful examination of the structures of the uncrept alloys was made using both optical microscopy and transmission electron microscopy.

Optical micrographs of the five alloys, both parallel and perpendicular to the plane of the sheet, are shown in Figures 3-7. The microstructures show that each alloy is partially recrystallized, with a high density of fine annealing twins. Since metallographic preparation of these materials is quite difficult, it is not possible to accurately measure the fraction recrystallized. However careful examination of microstructures (particularly those transverse to the plane of the sheet) allowed the following comparisons to be made.

(a) Alloys A and C, which contain 1 vol % ThO_2, have "recrystallized" structures which are nearly identical

(b) Alloys B and E are considerably less recrystallized, but their as-received structures are comparable

(c) Alloy D has a partially recrystallized structure intermediate between those of Alloys A and C, and B and E.

This distinction in as-received structure is important, since a comparison of the effects of particle size and spacing on creep rate is valid only if the initial structures are comparable.

Representative transmission electron micrographs (Figures 8-12) show the dislocation structures and the ThO_2 particle-size ranges and distributions. In all materials, the particles are uniformly dispersed with very little tendency for agglomeration. Even though Alloys B and E are considerably less recrystallized than Alloys A and C, the

*For the present alloys it was felt that transmission microscopy provided the most feasible means of obtaining accurate particle-size measurements. In the Appendix a comparison is made between transmission and replica microscopy techniques for particle-size measurements on Alloy B.

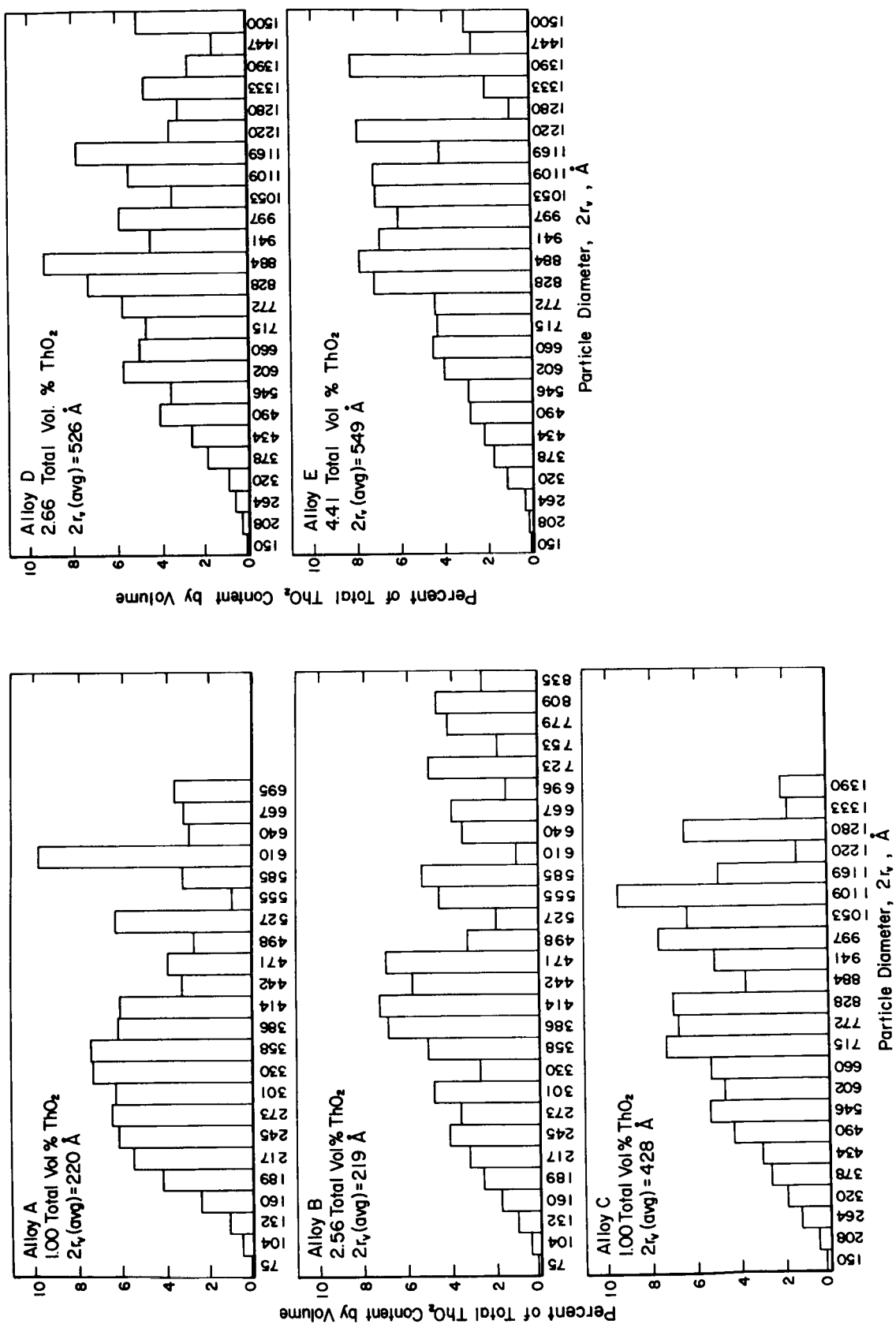

FIGURE 2. PARTICLE-SIZE DISTRIBUTION OF EXPERIMENTAL Ni-ThO_2 ALLOYS, EXPRESSED AS VOLUME PERCENT OF TOTAL ThO_2 CONTENT

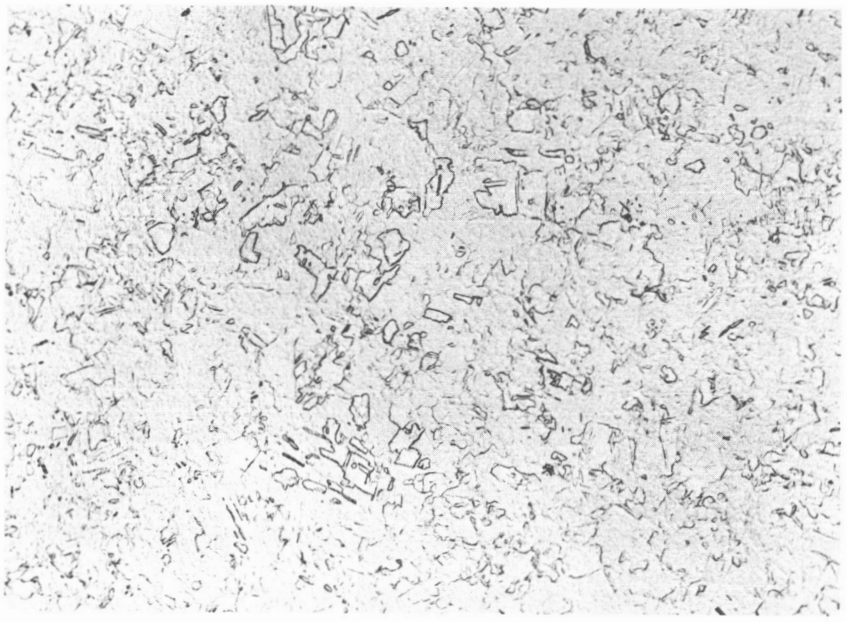

100X 29134

a. Surface

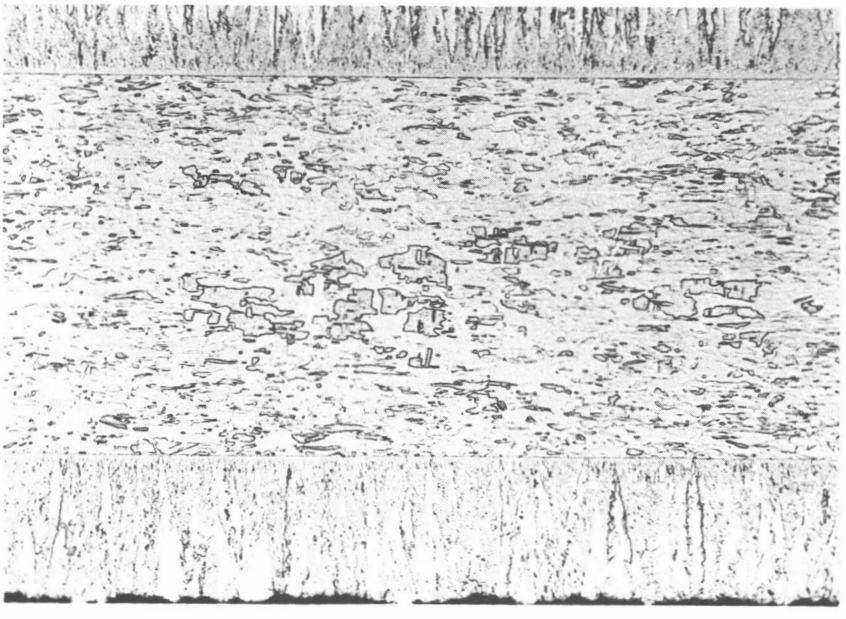

100X 28437

b. Transverse, Nickel Plated

FIGURE 3. MICROSTRUCTURE OF ALLOY A (Ni + 1.00 VOL % ThO_2, AVERAGE $2r_v$ = 220 Å, d = 2505 Å)

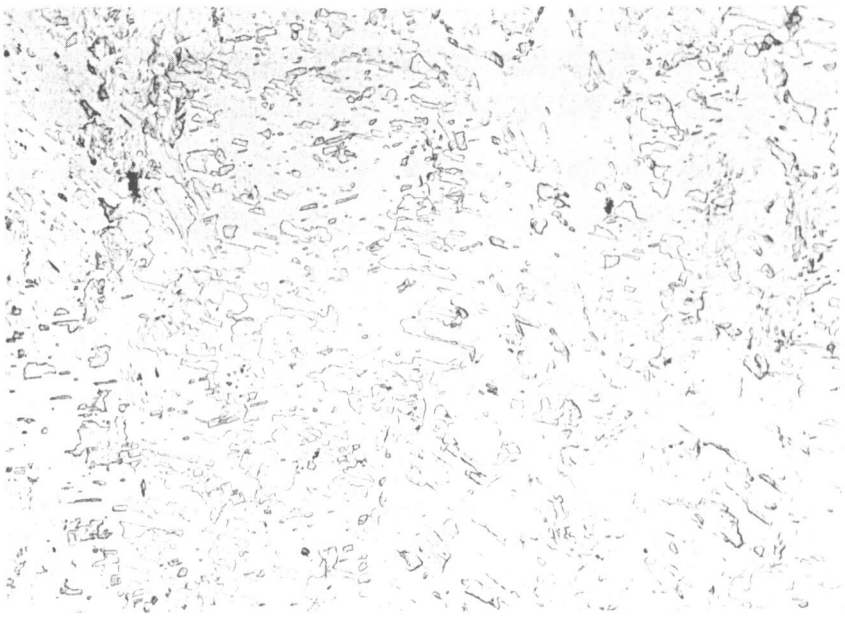

100X 29138

a. Surface

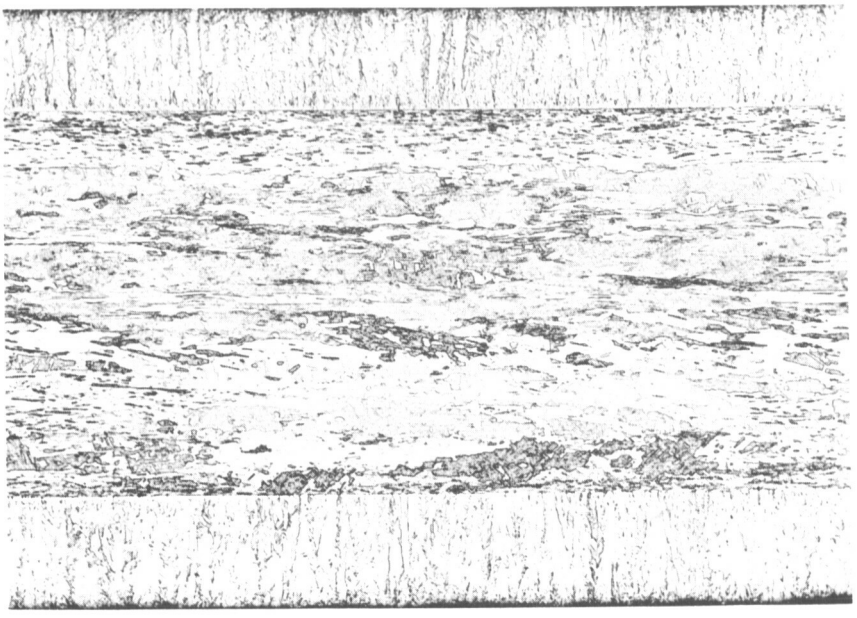

100X 28439

b. Transverse, Nickel Plated

FIGURE 4. MICROSTRUCTURE OF ALLOY B (Ni + 2.56 VOL % ThO_2, AVERAGE $2r_v$ = 219 Å, d = 1760 Å)

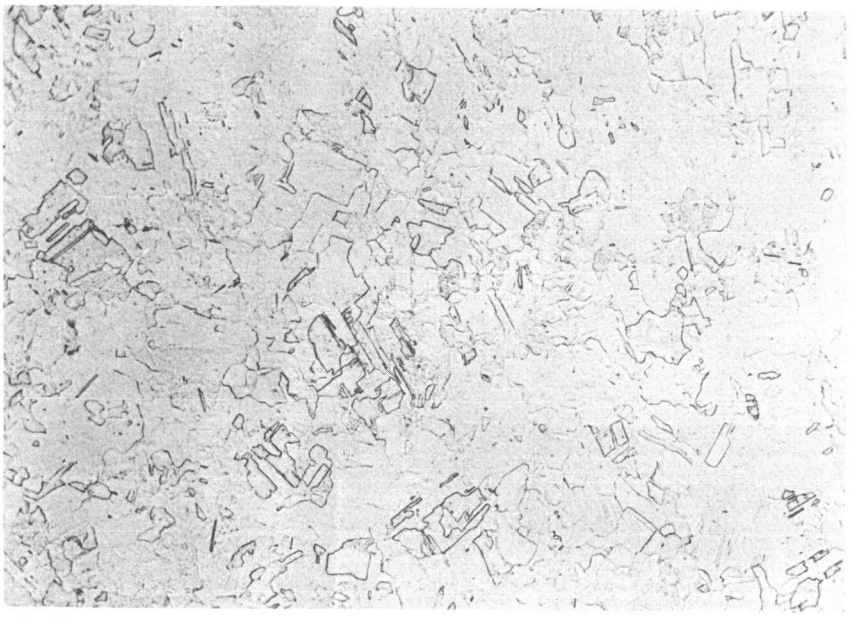

100X 29135

a. Surface

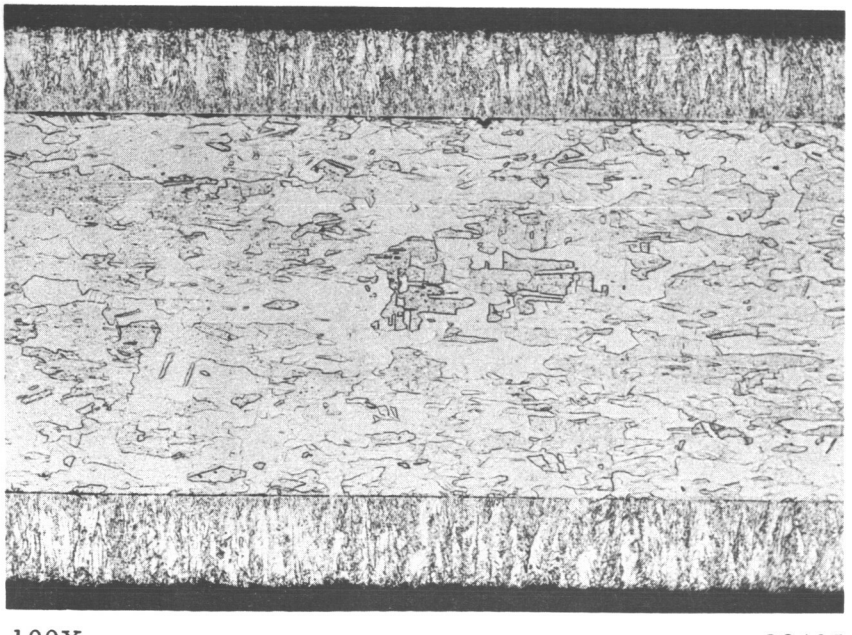

100X 28435

b. Transverse, Nickel Plated

FIGURE 5. MICROSTRUCTURE OF ALLOY C (Ni + 1.00 VOL % ThO_2, AVERAGE $2r_v$ = 428 Å, d = 5290 Å)

100X 29140

a. Surface

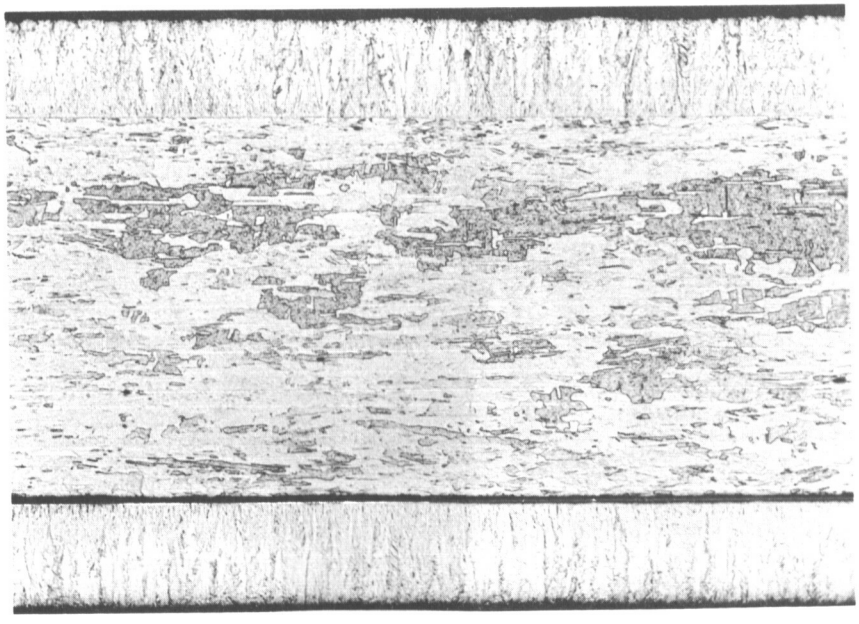

100X 28442

b. Transverse, Nickel Plated

FIGURE 6. MICROSTRUCTURE OF ALLOY D (Ni + 2.66 VOL % ThO_2, AVERAGE $2r_v$ = 526 Å, d = 3670 Å)

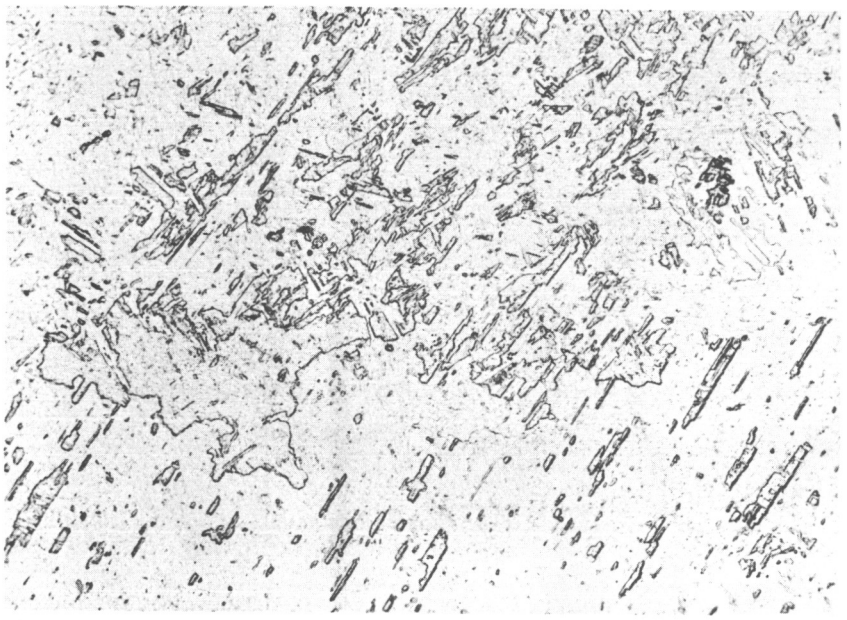

100X 29142

a. Surface

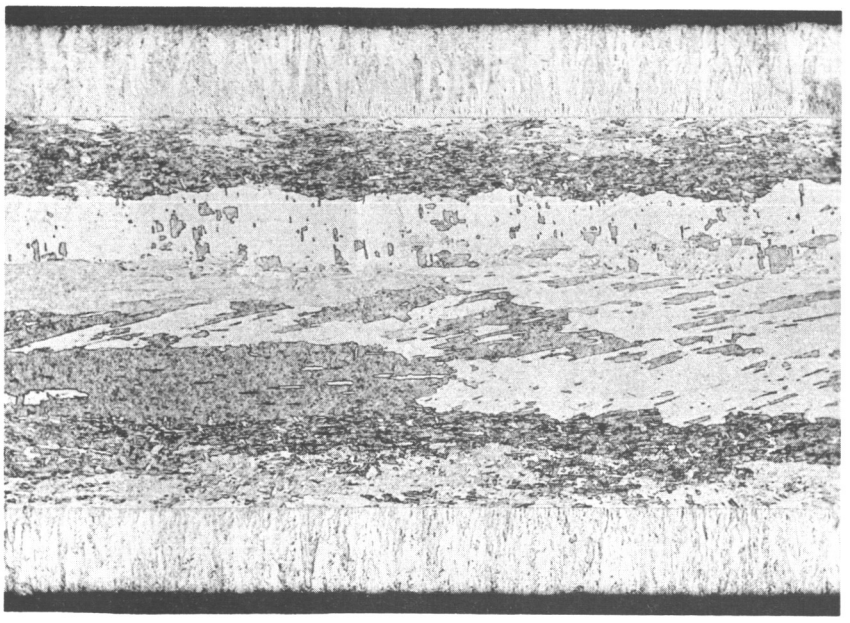

100X 28444

b. Transverse, Nickel Plated

FIGURE 7. MICROSTRUCTURE OF ALLOY E (Ni + 4.41 VOL % ThO_2, AVERAGE $2r_v$ = 549 Å, d = 2990 Å)

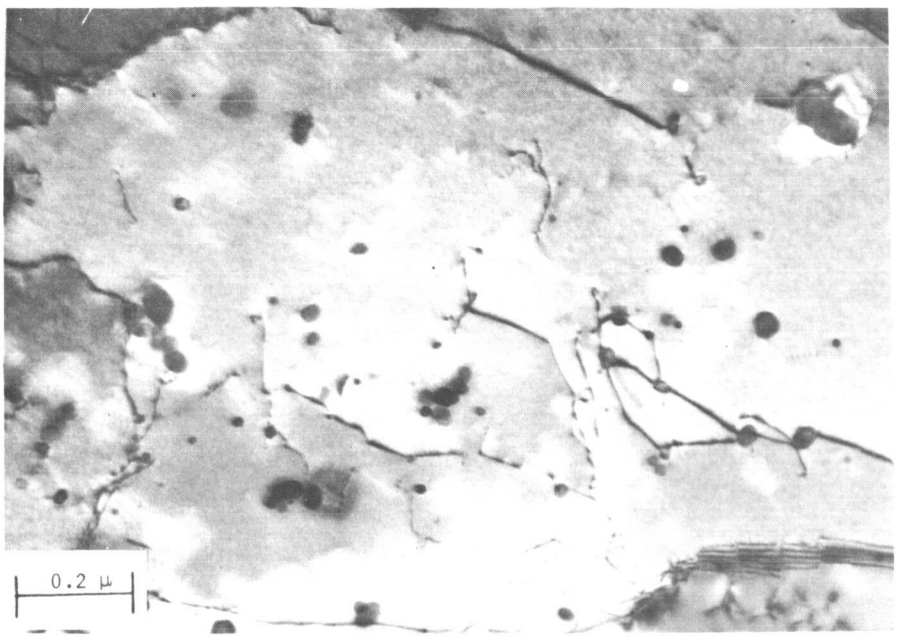

M035

a.

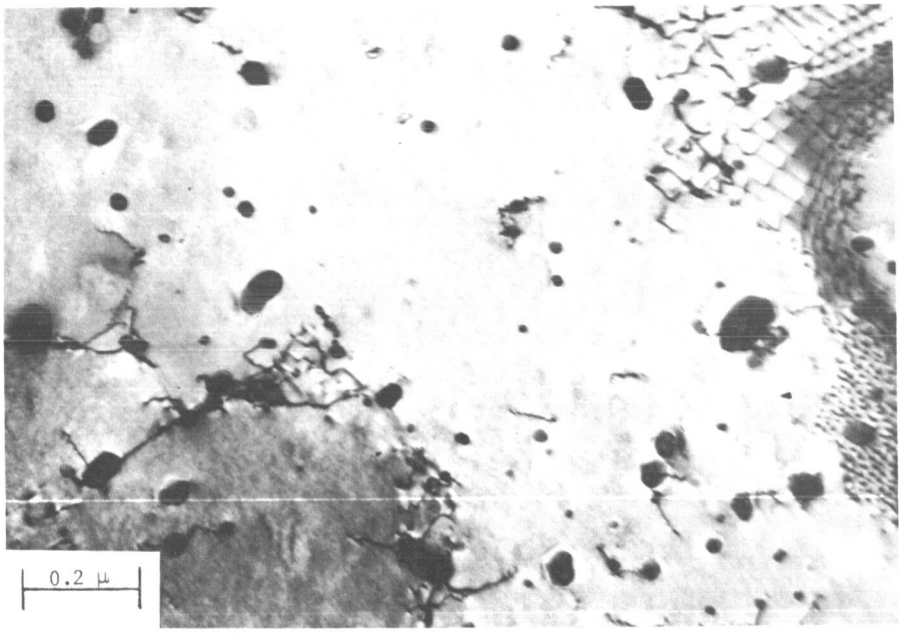

M008

b.

FIGURE 8. TRANSMISSION ELECTRON MICROGRAPHS OF AS-RECEIVED ALLOY A (Ni + 1 VOL % ThO_2, AVERAGE $2r_v$ = 220 Å, d = 2505 Å)

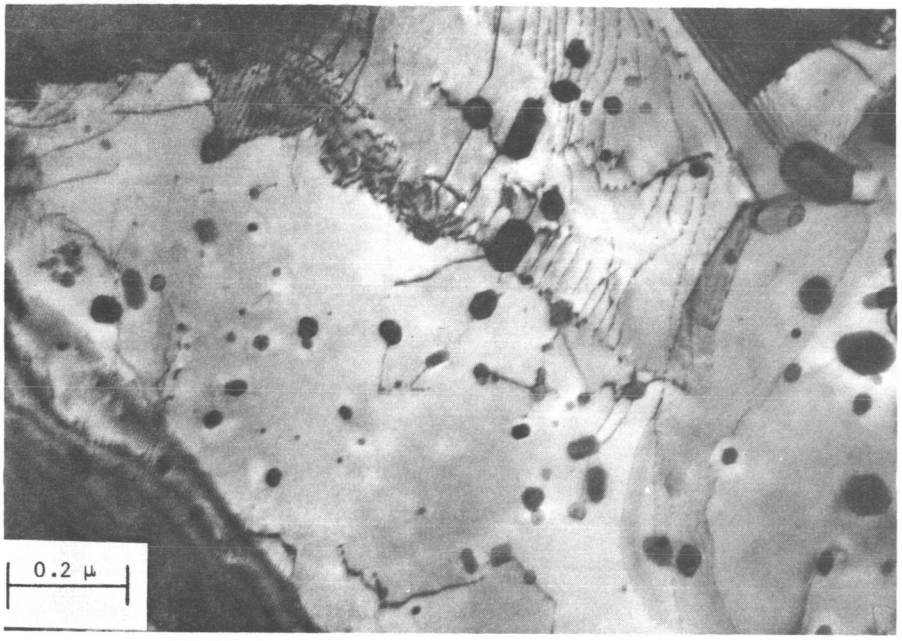

L222

a.

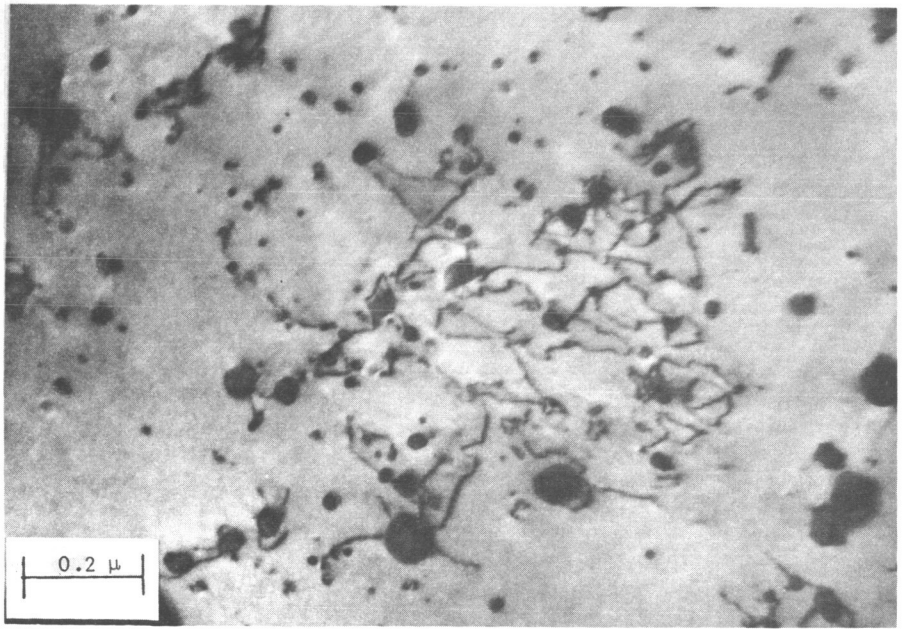

L239

b.

FIGURE 9. TRANSMISSION ELECTRON MICROGRAPHS OF AS-RECEIVED ALLOY B (Ni + 2.56 VOL % ThO_2, AVERAGE $2r_v$ = 219 Å, d = 1760 Å)

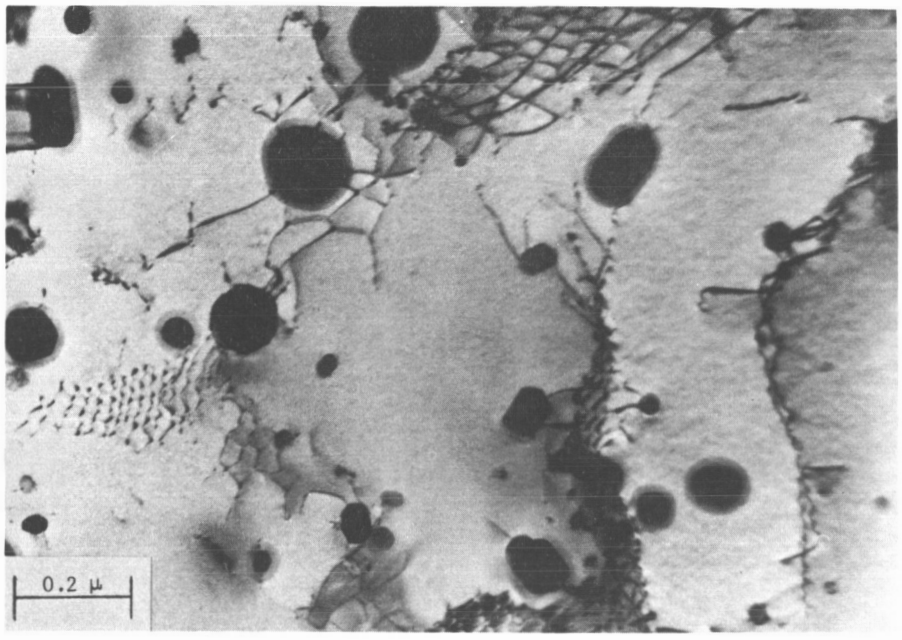

L089

a.

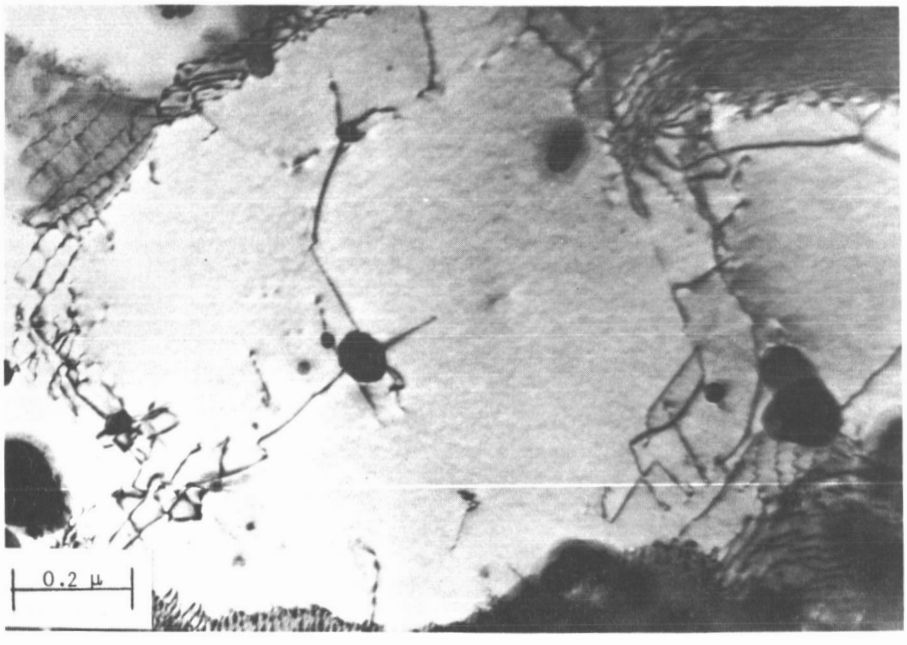

L095

b.

FIGURE 10. TRANSMISSION ELECTRON MICROGRAPHS OF AS RECEIVED ALLOY C (Ni + 1.00 VOL % ThO_2, AVERAGE $2r_v$ = 428 Å, d = 5290 Å)

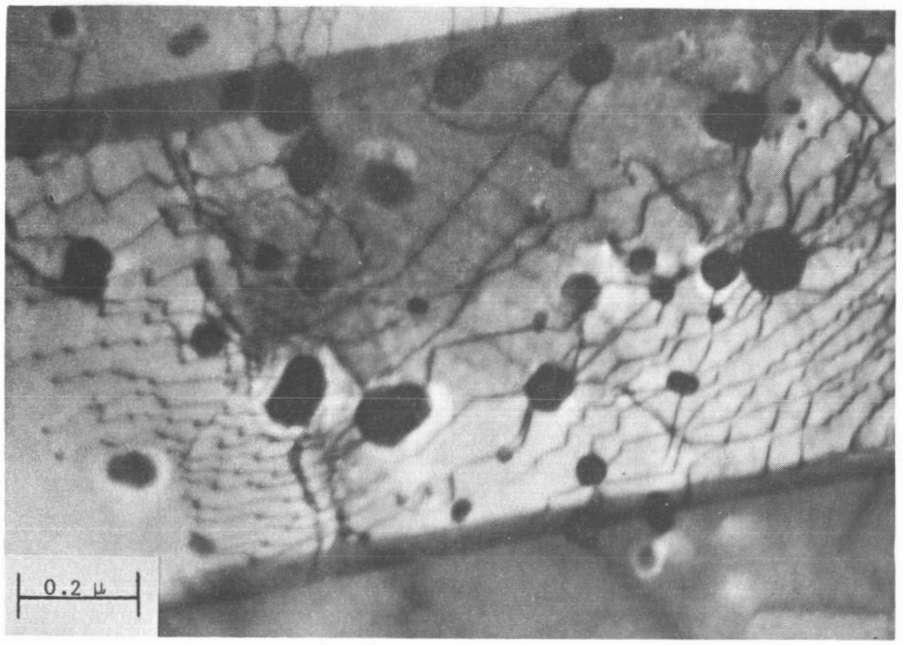

N116

a.

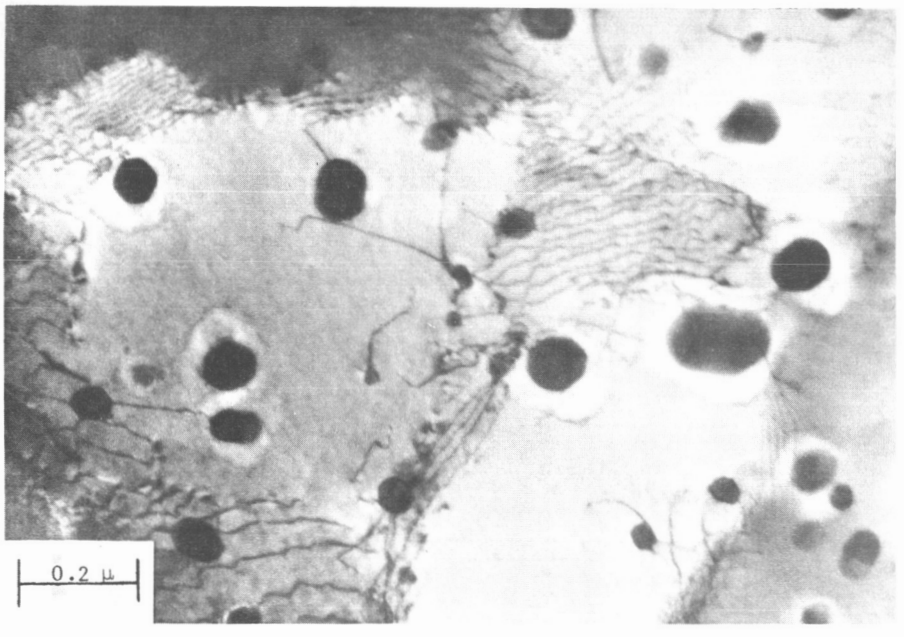

N141

b.

FIGURE 11. TRANSMISSION ELECTRON MICROGRAPHS OF AS-RECEIVED ALLOY D (Ni + 2.66 VOL % ThO_2, AVERAGE $2r_v$ = 526 Å, d = 3670 Å)

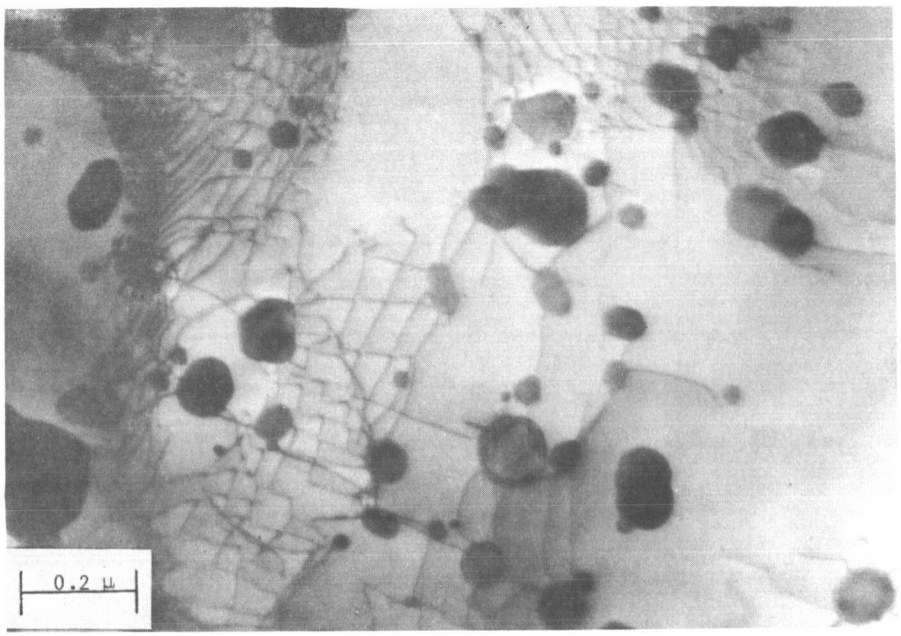

N146

a.

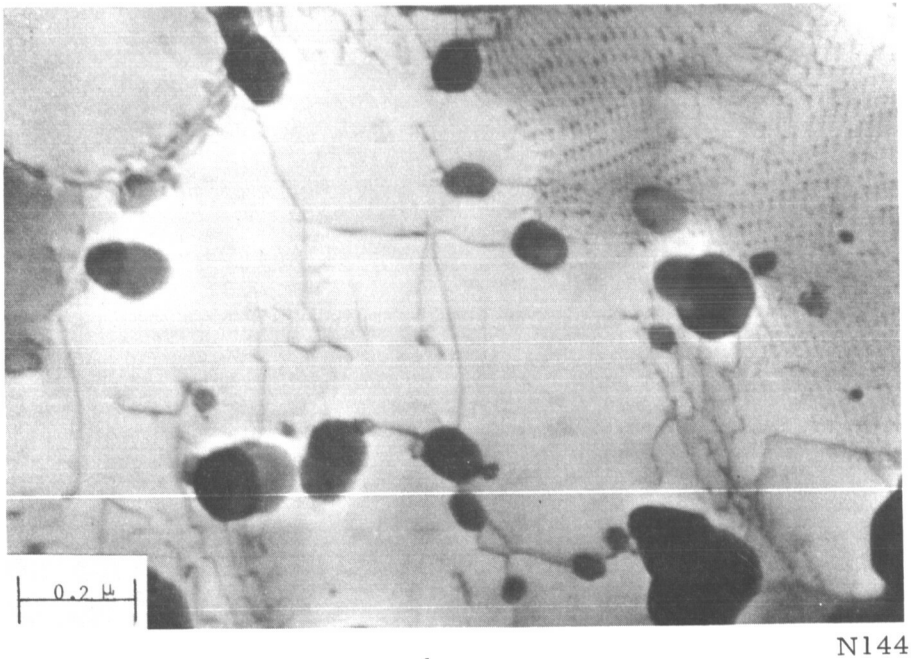

N144

b.

FIGURE 12. TRANSMISSION ELECTRON MICROGRAPHS OF AS-RECEIVED ALLOY E (Ni + 4.41 VOL % ThO_2, AVERAGE $2r_v$ = 549 Å, d = 2990 Å)

dislocation substructure of all the alloys is very similar. Several of the structural features which are common to each alloy are

(a) A dislocation substructure, composed of fine networks, is very predominant in nearly all foil areas. This probably occurred by climb recovery during the annealing cycles used in fabrication. Amelinckx[14] has reviewed the types of dislocation interactions that give rise to these network configurations.

(b) The annealing twins have a similar network structure. Figure 11a shows an example of this.

(c) Individual dislocations within the subgrains are strongly pinned by ThO_2 particles, i.e., very rarely did dislocations move within a thin foil.

RESULTS

Creep Studies

Results from creep tests indicate that the stress dependence and temperature dependence of the steady-state creep rate are considerably different from those previously observed on TD Nickel[8]. Typical creep curves, which are representative of all five alloys, are shown in Figure 13, and the creep data are listed in Table 4. The effect of temperature on the steady state creep rate is illustrated in Figure 14, where for each of the alloys log ($\dot{\epsilon}_s$ T) is plotted as a function of reciprocal absolute temperature. Parallel lines were drawn which best fit the data for each of the alloys, and the calculated activation energy for creep, Q_c, was 64 kcal/mole. This value is within the range of reported values for Q_{sd} in nickel[15] (61-67 kcal/mole) and agrees with the activation energy for creep of pure polycrystalline nickel[16] (65 kcal/mole).

The stress dependence of $\dot{\epsilon}_s$ can be reasonably represented by a power law, $\dot{\epsilon}_s \propto \sigma^m$ where m has a value of ~7. This is demonstrated in Figure 15 where the temperature-compensated creep rate is plotted as a function of log σ. There appears to be some precedence for a stress exponent of ~7 obtained from high temperature creep tests of dispersion strengthened alloys. Takahashi, et al.,[17] determined m values of 6.2-7.9 for Ni + 3 wt % Al_2O_3 and Ni + 5 wt % Al_2O_3 crept over the temperature range 650-800°C. Also the creep data of Ansell and Lenel[7] on a recrystallized SAP-type alloy tested at 600 and 620°C (i.e., these were their lower stress tests) can be treated to produce a stress exponent of ~7 to 8.

The creep results of these alloys, therefore, can be represented by an equation of the form:

$$\dot{\epsilon}_s = \frac{C}{T} \sigma^m \exp - \left(\frac{Q_c}{RT}\right) \quad , \tag{5}$$

where C is a constant for a given alloy, and the experimental values of m and Q_c are ~7 and 64 kcal/mole respectively. The data in Figure 15 indicate that Q_c is stress independent over the ranges of stress investigated.

TABLE 4. STEADY-STATE CREEP RATE AS A FUNCTION OF TEMPERATURE AND APPLIED STRESS

Alloy	σ, psi	T, °C	$\dot{\epsilon}_s$, sec^{-1}	Alloy	σ, psi	T, °C	$\dot{\epsilon}_s$, sec^{-1}
A	7,000	700	2.17×10^{-7}	D	8,000	800	1.39×10^{-7}
A	6,000	725	2.17×10^{-7}	D	6,000	850	6.21×10^{-8}
A	5,000	775	2.20×10^{-7}	D	5,500	850	3.68×10^{-8}
A	4,000	875	7.12×10^{-7}	D	5,000	850	9.49×10^{-9}
A	4,000	850	3.38×10^{-7}	D	4,000	950	8.57×10^{-8}
A	4,000	825	2.33×10^{-7}	D	4,000	925	4.85×10^{-8}
A	4,000	800	1.00×10^{-7}	D	4,000	900	3.14×10^{-8}
A	2,000	950	1.97×10^{-8}	D	4,000	850	6.50×10^{-9}
				D	3,000	950	3.98×10^{-9}
B	17,000	900	(a)				
B	15,000	900	(a)	E	9,000	750	3.97×10^{-10}
B	15,000	850	1.18×10^{-7}	E	8,000	950	(a)
B	12,000	825	1.21×10^{-8}	E	8,000	925	1.01×10^{-8}
B	12,000	800	4.72×10^{-9}	E	8,000	900	4.32×10^{-9}
B	12,000	785	5.66×10^{-9}	E	8,000	875	2.18×10^{-9}
B	12,000	760	2.56×10^{-9}	E	8,000	850	1.30×10^{-9}
B	12,000	720	4.02×10^{-10}	E	7,000	1000	(a)
B	7,000	1000	(b)	E	6,000	850	3.18×10^{-10}
B	6,000	950	2.61×10^{-9}	E	4,000	1000	4.32×10^{-10}
B	4,000	1050	8.30×10^{-10}				
C	12,000	750	(a)				
C	12,000	700	3.00×10^{-7}(c)				
C	8,000	700	3.59×10^{-8}(c)				
C	8,000	650	8.65×10^{-9}(d)				
C	8,000	600	1.73×10^{-9}(d)				
C	6,000	725	(b)				
C	6,000	675	6.10×10^{-8}				
C	4,000	800	2.42×10^{-7}				
C	4,000	770	6.47×10^{-8}				
C	4,000	750	5.20×10^{-8}				
C	4,000	725	2.47×10^{-8}				
C	4,000	715	1.63×10^{-8}				
C	3,000	900	3.95×10^{-7}				
C	2,000	900	2.24×10^{-8}				

(a) Failed on loading.

(b) Specimen undercut causing local deformation where shoulder radius meets gage length. Thus true gage length is unknown and $\dot{\epsilon}_s$ could not be determined.

(c) Rupture life less than 5 hours – possibly no true steady-state creep region. Data do not fit plot in Figure 15.

(d) Lowest test temperatures for this alloy. Data do not fit curve in Figure 15. May possibly be associated with low-temperature creep mechanism.

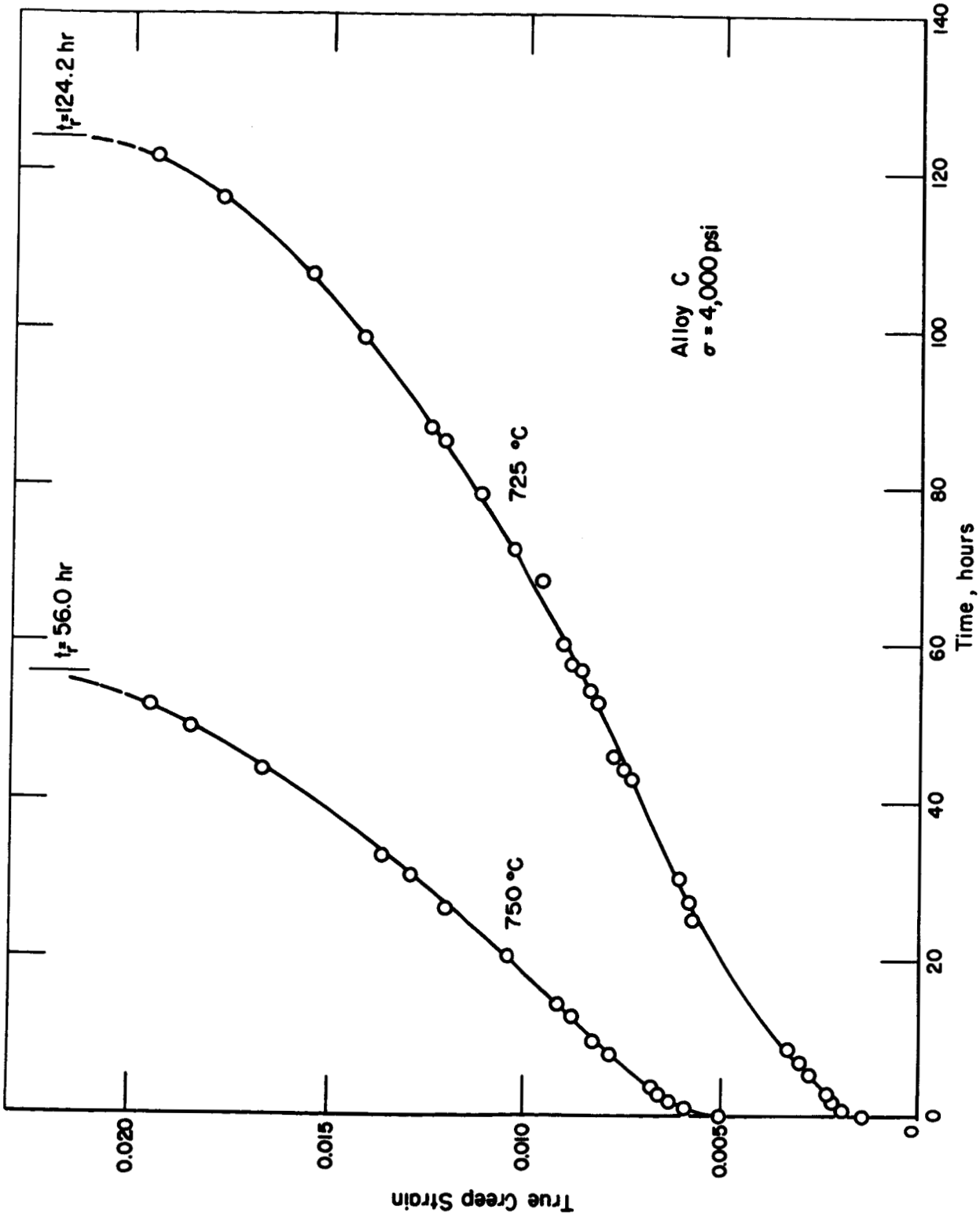

FIGURE 13. TYPICAL CREEP CURVES, REPRESENTATIVE OF THE EXPERIMENTAL Ni-ThO_2 ALLOYS

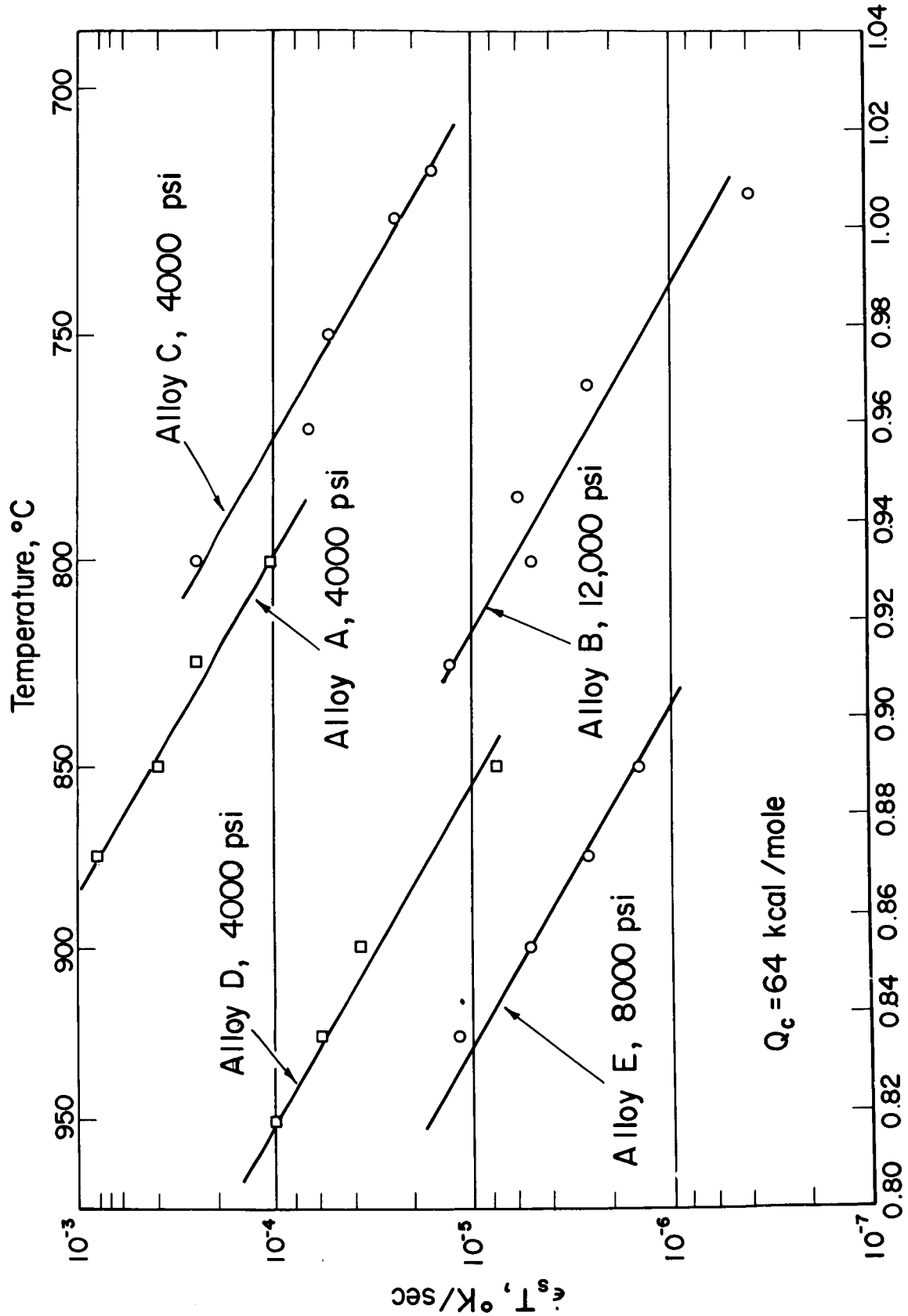

FIGURE 14. TEMPERATURE DEPENDENCE OF THE STEADY-STATE CREEP RATE

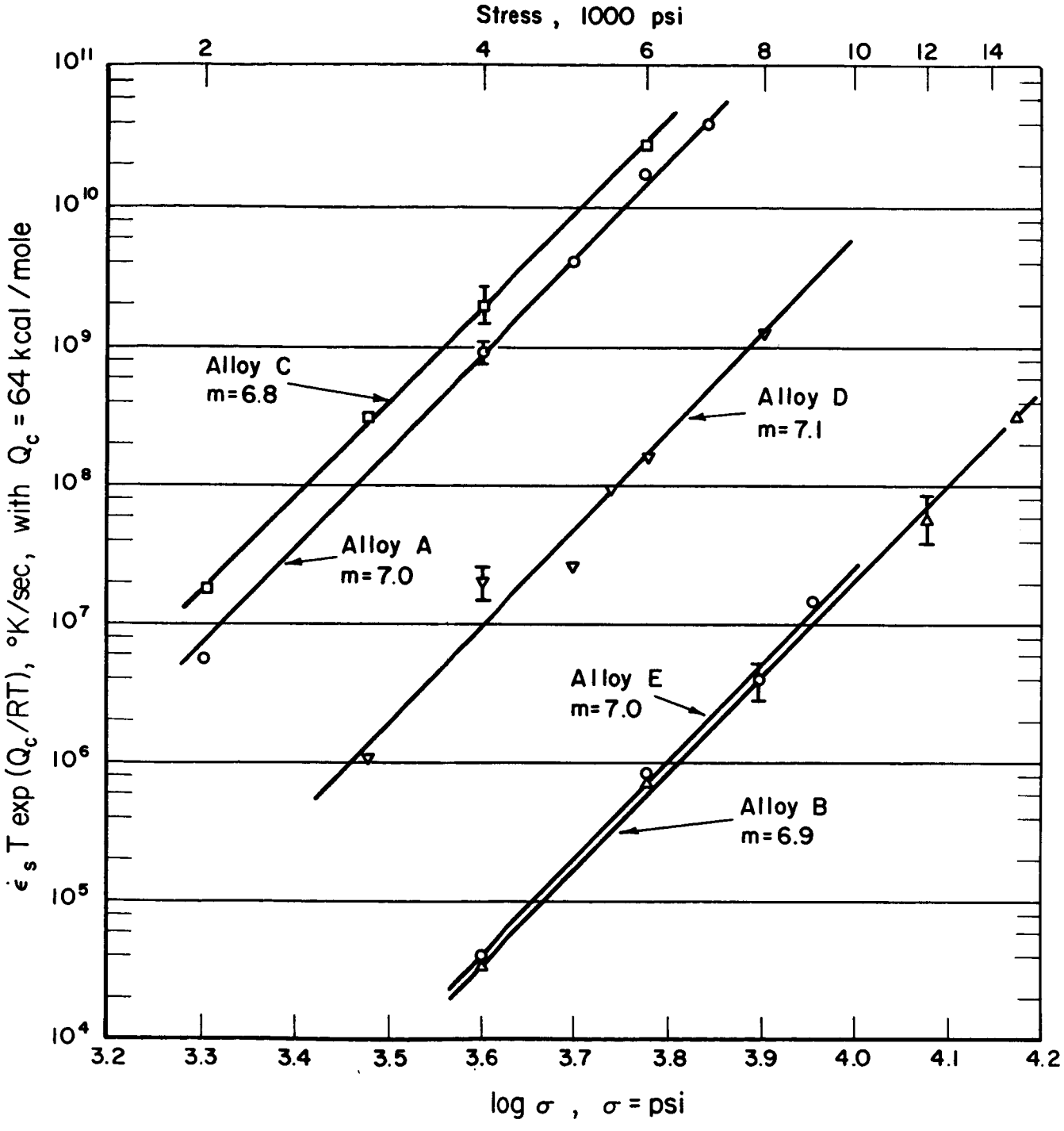

FIGURE 15. STRESS DEPENDENCE OF THE TEMPERATURE-COMPENSATED CREEP RATE

The dislocation substructure generated during high-temperature creep is shown in Figures 16 and 17. The foils for electron microscopy were taken ~5 mm from the fracture and thus were in the uniformly deformed section of the gage lengths. The creep strain in these areas was ~1-1.2 percent. The structures in Figures 16 and 17 show the same dislocation networks as were noted in uncrept specimens, although qualitatively they appear to be slightly more extensive in crept specimens. The chief difference in the crept structure is the higher density of jogged dislocations within the subgrains (see especially Figure 17b). Occasionally, areas of heavy tangling of the jogged dislocations are noted (see A in Figure 16b).

Stress Dependence of the Dislocation Density Generated During Creep

Previous investigators have reported that the total dislocation density, ρ_T, generated during high-temperature creep of iron[18] and Fe-3% Si[19] is approximately proportional to $\sigma^{1.4}$, where σ is the applied stress. Thus a portion of the stress dependence of the steady-state creep rate may be associated with the effect of stress on dislocation density. In an effort to determine if there were an effect of stress on dislocation density in the Ni-ThO_2 alloys, ρ_T measurements were made on one alloy (Alloy D) crept at 850°C and four stresses (4,000, 5,000, 5,500, and 6,000 psi). The specimens were crept into the steady-state region and cooled under load. The total creep strain in each case was ~1.2 percent.

Thin foils were prepared from the crept specimens, and typical structures are shown in Figure 18. Dislocation density measurements were made using the lineal count technique described by Ham[20]. This method gives ρ_T as:

$$\rho_T = \frac{2N'M}{Lt} \quad , \tag{6}$$

where L is the total length of a set of random lines drawn on a micrograph, N' is the number of intersections which dislocations make with the set of grid lines, t is the foil thickness, and M is the plate or print magnification. When making the dislocation counts, measurements were made on only those dislocations not in subgrain boundaries. This arbitrary selection was invoked because the sub-boundaries were also present in uncrept specimens, and it was impossible to quantitatively determine any changes in density within the boundaries as a result of creep.

This variation of ρ_T with applied creep stress is shown in Figure 19. Each data point reflects the average of 15-20 micrographs, with ~10 counts per micrograph. It is noted that there is considerable scatter in the data; however, the stress dependence of ρ_T is shown to be approximately $\rho_T \propto \sigma^{\beta}$, where $\beta = 1.8$. These results are in accordance with previous creep studies on Fe[18] and Fe-3% Si[19], where β was found to be 1.4.

Fracture Studies

Micrographs in Figure 20 show the typical fracture appearance of the Ni-ThO_2 alloys. The fracture is ductile, and numerous internal cavities are noted both near the

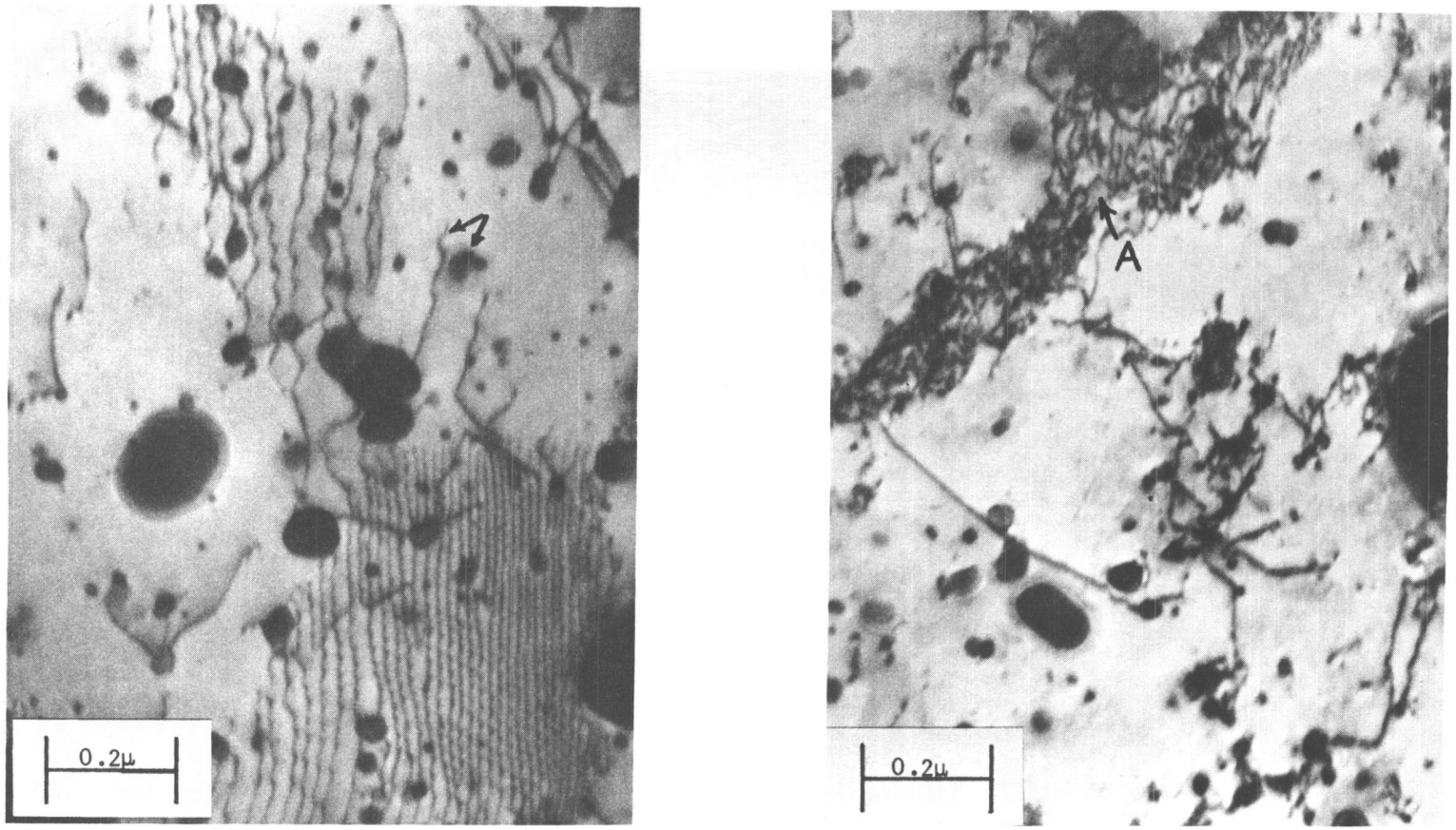

P167 (a)

Q250 (b)

FIGURE 16. STRUCTURE OF A CREPT SPECIMEN OF ALLOY B; σ = 12,000 PSI, T = 825°C

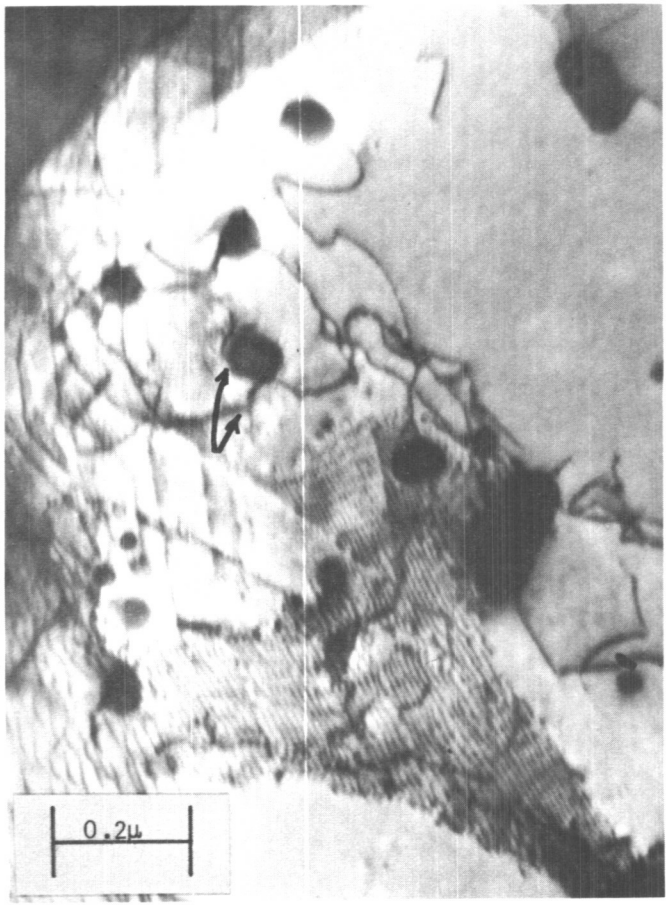

Q312

(a)

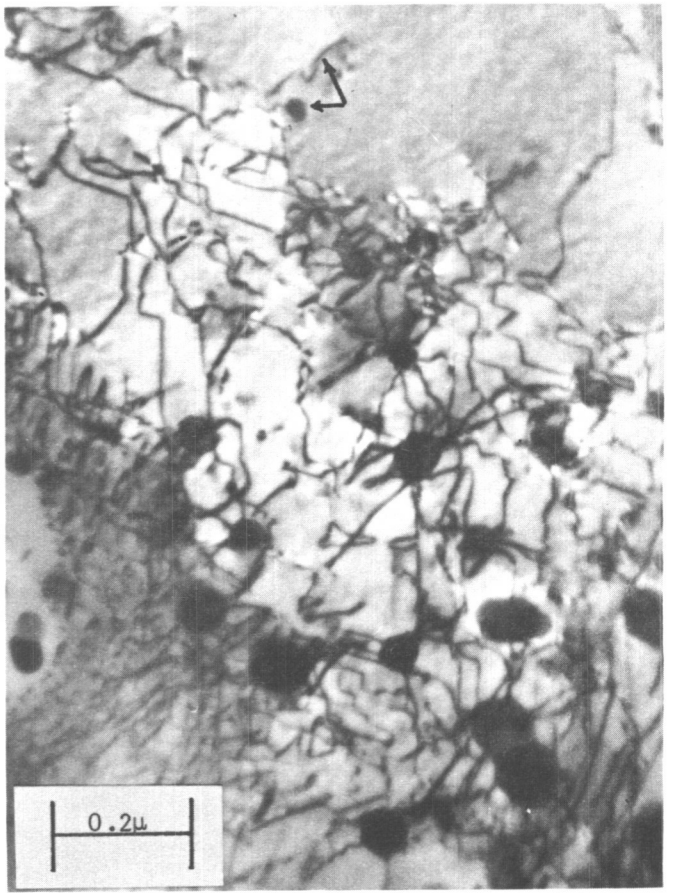

Q260

(b)

FIGURE 17. STRUCTURE OF A CREPT SPECIMEN OF ALLOY C; σ = 4,000 PSI, T = 800°C

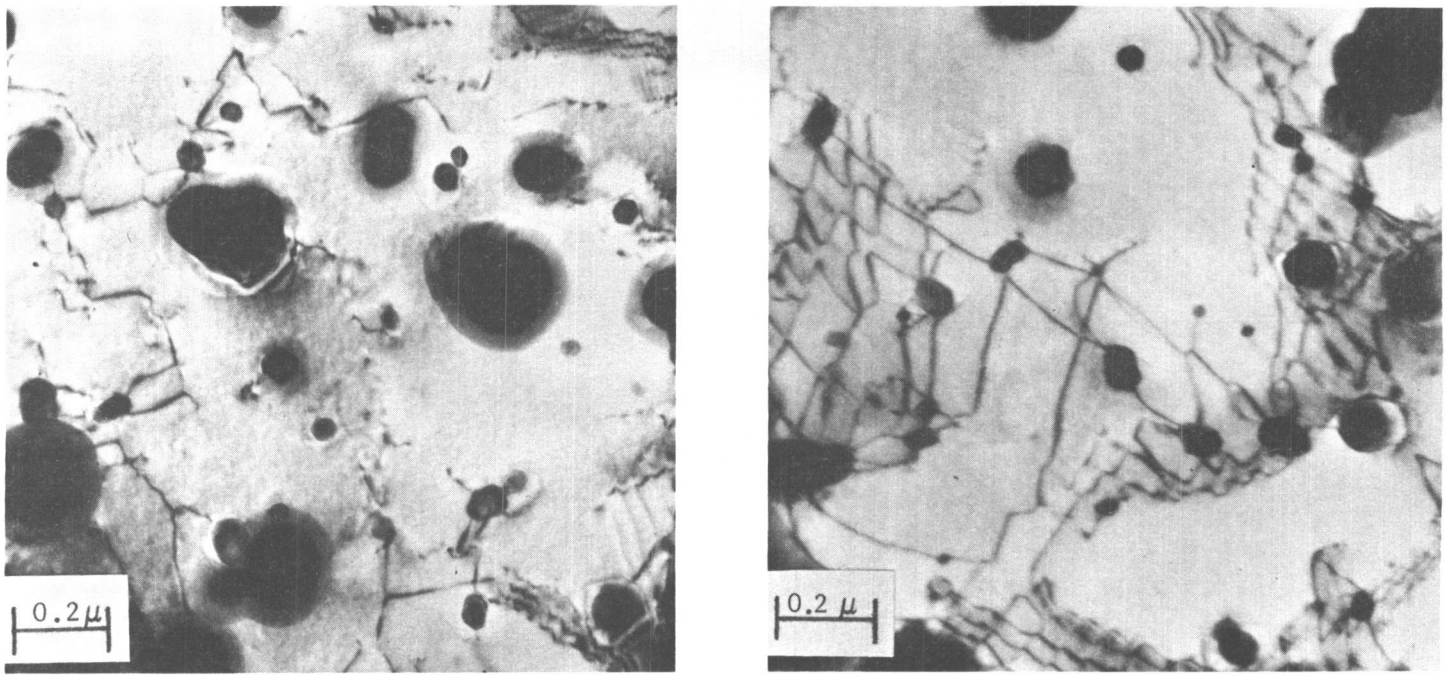

E2060B

a. σ = 4,000 psi

E2059D

b. σ = 6,000 psi

FIGURE 18. TYPICAL STRUCTURES OF ALLOY D, CREPT AT 850°C AND DIFFERENT STRESSES

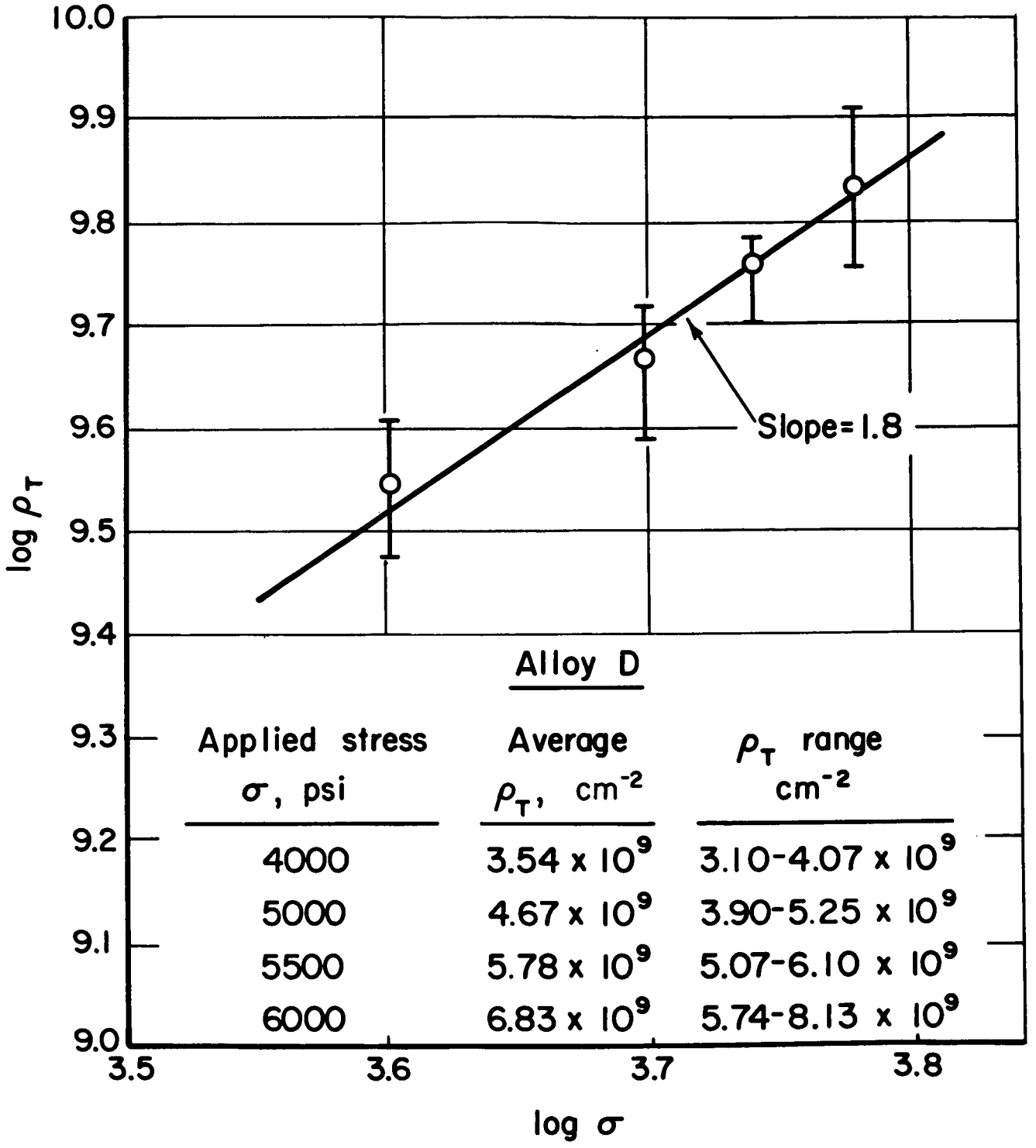

FIGURE 19. STRESS DEPENDENCE OF THE DISLOCATION DENSITY IN SPECIMENS OF ALLOY D CREPT AT 850°C (see text for definition of ρ_T). IN UNCREPT SPECIMENS THE DISLOCATION DENSITY WITHIN THE SUBGRAINS WAS ~$10^9 cm^{-2}$

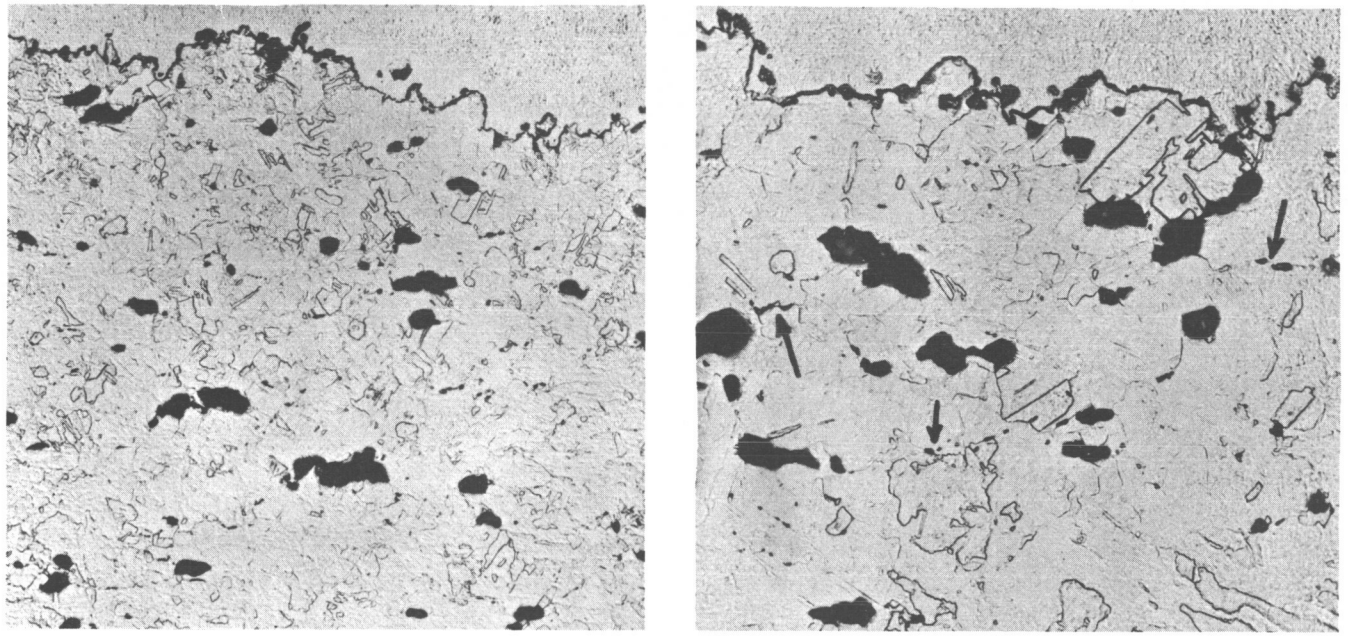

100X 6A039 (a)

250X 6A043 (b)

FIGURE 20. MICROGRAPHS SHOWING TYPICAL FRACTURE APPEARANCE, ALLOY A, TESTED AT 825°C AND 4,000 PSI, FRACTURE SURFACE IS NICKEL PLATED, AND STRESS AXIS IS VERTICAL

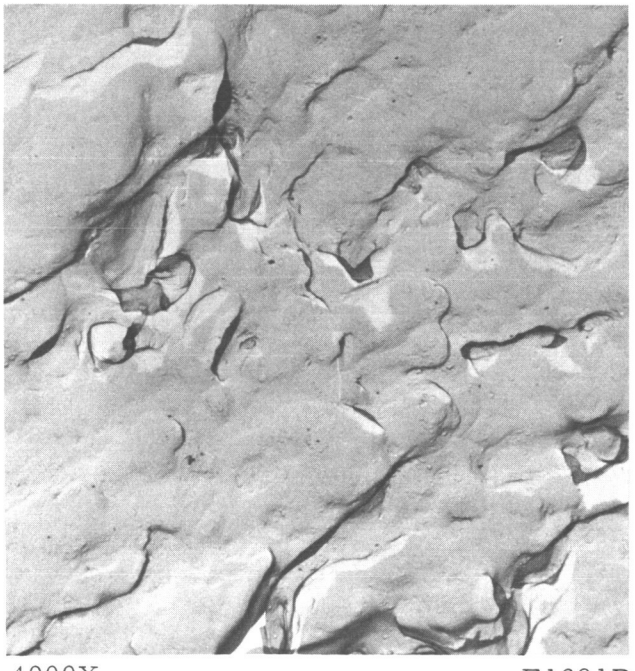

4000X E1391D

FIGURE 21. REPLICA FRACTOGRAPH OF ALLOY A, CREPT TO FAILURE AT 825°C AND 4,000 PSI

fracture and along the entire specimen gage length. The fracture appearance is typical of those commonly observed in high-temperature creep fractures of polycrystalline metals[21]. The cavities are nucleated on grain boundaries (see arrows in Figure 20b), and void enlargement probably occurs, at least in part, by plastic tearing[22]. The fracture surface (Figure 21) has a scalloped appearance, with ThO_2 particles occasionally exposed.

DISCUSSION

In the following discussion a dislocation climb model similar to that of Ansell and Weertman[4] is developed and applied to the creep results on the experimental Ni-ThO_2 alloys. Although the physical picture adopted is similar to that described by Ansell and Weertman, the derivation differs from theirs in that a different stress dependence of $\dot{\epsilon}_s$ is predicted. This arises from the consideration that the density of mobile edge dislocations is stress dependent. In addition, part of the stress dependence of $\dot{\epsilon}_s$ is associated with the internal stress, σ_i, due to the precreep substructure. That is, any formulation including stress should be expressed as the effective stress, σ_e, rather than the applied stress, σ, (i.e., $\sigma_e = \sigma - \sigma_i$).

The Climb Model

As mentioned in the Introduction, the formalism of a climb model depends on the level of stress. A low-stress model is applicable when treating the present results since the applied stresses were insufficient to cause dislocations to bow to the minimum radius and pinch off by the Orowan mechanism. This is shown in Table 5 where the applied shear stresses are noted to be less than the Orowan bowing stress, τ_P, calculated from the relation given by Kelly and Nicholson[1]:

$$\tau_P = \frac{\mu b}{4\pi} \frac{2}{(d - 2r_s)} \phi \ln\left(\frac{d - 2r_s}{2b}\right) . \qquad (7)$$

Here, $\phi \simeq 1.25$ is an averaging factor for the screw-edge character of the bowed-out loop, and d and $2r_s$ are defined in Table 2. The shear modulus of the matrix, μ, was compensated for temperature as described in Reference 8.

Since the activation energy for creep is equal to that for self-diffusion in nickel and also appears to be stress independent over the range of stresses applied to the alloys it is probable that the movement of jogged screw dislocations is not the rate-controlling mechanism here. In fact, it is likely that in this temperature range the screw dislocations easily bypass the particles by cross-slip and are relatively unrestricted in their motion compared to the edge dislocations. Therefore, the physical model adopted is one of the edge dislocations being held up at particles[4], with the rate-controlling process being climb over the particles. This is shown in Figure 22 where a sequence of climb events is schematically illustrated. Enhanced local climb can result from the close proximity of the pinned segment to the particle/matrix interface which may act as a potent source or sink of vacancies. There is some evidence from electron micrographs on crept specimens that dislocation-particle configurations resembling those in Figure 22 are developed during creep. For example, in Figures 16 and 17, arrows indicate

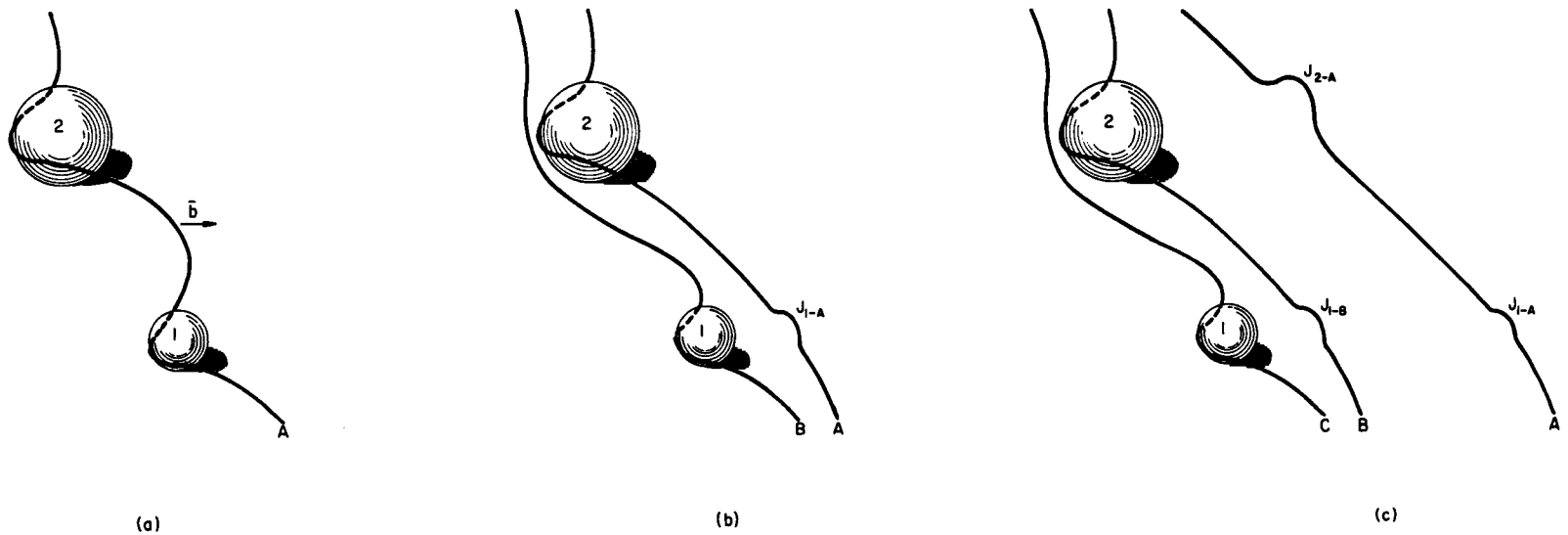

FIGURE 22. SCHEMATIC VIEW (THREE DIMENSIONAL) OF DISLOCATIONS BOWING AROUND AND CLIMBING OVER SPHERICAL PARTICLES

The sequence of events is

(a) Dislocation A is slightly bowed around particles 1 and 2.

(b) Dislocation A has climbed over particle 1 leaving a climb jog, J_{1-A}, but is still blocked by particle 2. Dislocation B has arrived and is bowed around particle 1.

(c) Dislocation A has now climbed past particle 2, and has two climb jogs, J_{1-A} and J_{2-A}. Dislocation B has climbed over particle 1, etc.

dislocations which possibly contain climb jogs, and the particles that they may have climbed over.

TABLE 5. COMPARISON OF THE OROWAN STRESS AND THE APPLIED STRESS FOR THE FIVE EXPERIMENTAL ALLOYS

Alloy	τ_p, psi	τ Applied[(a)], psi
A	11,400	3,500
B	15,700	7,500
C	6,100	3,000
D	8,600	4,000
E	10,600	4,500

(a) This is the maximum applied creep stress for each alloy (see Figure 15) and is calculated as one-half the applied tensile stress. The effective shear stress acting on a bowed loop will be less than τ applied because of the internal stress, τ_i.

The steady state creep rate, $\dot{\epsilon}_s$, is given by,

$$\dot{\epsilon}_s = NAbR \quad , \tag{8}$$

where N = number of points per unit volume at which climb of edge dislocations over particles can occur, A = area swept out by a dislocation after climbing over a particle, b = Burgers vector, and R = rate at which the particles are surmounted, i. e., the climb rate.

The quantity N is a function of both the density of mobile edge dislocations within the subgrains, ρ_{em}, and the spacing, $\bar{x}$, between the effective pinning points.

$$N = \frac{\rho_{em}}{\bar{x}} \tag{9}$$

For low stresses, such as those used in the present study, this spacing is approximated by λ, the mean free path [$\lambda = 4r_v(1-f)/3f$, where f = volume fraction of the dispersed phase][(23)]; whereas for higher stresses the spacing would be closer to d, the mean planar center-to-center particle spacing. The values of λ for the experimental alloys are Alloy A, $\lambda \simeq 1.5\ \mu$; Alloy B, $\lambda \simeq 0.6\ \mu$; Alloy C, $\lambda \simeq 2.8\ \mu$; Alloy D, $\lambda \simeq 1.3\ \mu$; Alloy E, $\lambda \simeq 0.8\ \mu$.

Experimental measurements of the dependence of the total dislocation density, ρ_T, on applied (tensile) creep stress indicated that $\rho_T = \text{const.}\ \sigma^\beta$, where $\beta \simeq 2$ (see Figure 19). If it assumed that the density of mobile edge dislocations is similarly influenced by stress, then

$$\rho_{em} \simeq \rho_o \sigma^2 \quad , \tag{10}$$

where ρ_o is a constant. Thus N is given by,

$$N \simeq \frac{\rho_o \sigma^2}{\lambda} \quad . \tag{11}$$

In Equation (8) the area swept out by a dislocation segment each time it climbs over a particle is approximated by

$$A \simeq d^2 \quad . \tag{12}$$

The climb rate, R, is taken to be

$$R = \frac{2\sigma^2 \, b \, d \, D}{r_v \, \mu \, kT} \quad , \tag{13}$$

where k is Boltzman's constant and D is the volume self-diffusivity in the matrix and is equal to $D_o \exp(-Q_{sd}/RT)$. Equation (13) is essentially that derived by Ansell[2] for the case where there are dislocation pile-ups behind particles. Kocks[25] has recently examined the consequences of a random distribution of point-like obstacles on the movement of dislocations. Based on his statistical analysis, it is reasonable to expect that limited pile-ups will occur by glide in dispersion-hardened alloys such as those in this investigation.

Substituting Equations (11), (12), and (13) into Equation (8) gives the steady-state creep rate as

$$\dot{\epsilon}_s = \frac{K \sigma^4 \, d^3 \, b^2}{\lambda \, r_v \, \mu \, T} \exp - \left(\frac{Q_{sd}}{RT}\right) \quad , \tag{14}$$

where $K = 2\rho_o D_o/k$. For unresolved stress and strain rate the right-hand side of Equation (14) should be divided by $16\sqrt{2}$. At higher stresses, $\bar{x}$ in Equation (9) is given by d rather than λ, and then $\dot{\epsilon}_s \propto d^2/r_v$.

In Equation (14) $\dot{\epsilon}_s \propto \sigma^4$, whereas it was found that the experimental stress exponent was $m \simeq 7$ (see Figure 15). This discrepancy can be rationalized, at least in part, by noting that in Equation (14) the stress is really the effective stress $\sigma_e = \sigma - \sigma_i$, whereas $m \simeq 7$ was determined from a log-log plot of temperature compensated creep rate versus applied stress. Thus the stress exponent in Equation (14) should be less than 7 since $\sigma_e < \sigma$. The reduced exponent can be written in terms of m and $(\sigma - \sigma_i)$ in the manner proposed by Takahashi, et al.,[17]*.

$$4 = m \left[\frac{\Delta \log \sigma}{\Delta \log (\sigma - \sigma_i)}\right] = m \left[\frac{\log (\sigma_1/\sigma_2)}{\log \left(\frac{\sigma_1 - \sigma_i}{\sigma_2 - \sigma_i}\right)}\right] \tag{15}$$

An estimate can be made of the internal stress σ_i for the various alloys by applying Equation (15) to the data in Figure 15, and the results of such calculations are given in Table 6. The values of σ_i are reasonable, and for each alloy σ_i is lower than the lowest applied creep stress. The comparative values of σ_i also agree qualitatively with the as-received structures (see Figures 3-7). Alloys A and C have nearly identical "recrystallized" structures and have the lowest σ_i values. Alloys B and E are considerably less recrystallized and, in turn, have the highest values of internal stress.

*The applied stresses, σ_1 and σ_2, used from Figure 15 were the highest and lowest experimental stresses for each alloy.

TABLE 6. VALUES OF THE INTERNAL STRESS, σ_i, CALCULATED FROM EQUATION (15) AND FIGURE 15

Alloy	Experimental Stress Exponent, m	σ_i, psi	Lowest Applied Stress, psi
A	7.0	1300	2000
B	6.9	2900	4000
C	6.8	1100	2000
D	7.1	1900	3000
E	7.0	2900	4000

Equation (14) predicts that the particle parameters influence the steady-state creep rate as $\dot{\epsilon}_s \propto d^3/\lambda r_v$. Thus it is possible to compare experimental and calculated creep rate ratios of various alloys at constant stress and temperature, provided the alloys have equivalent initial microstructures (i. e., equivalent values of σ_i). Such comparisons are legitimate for: Alloy A with Alloy C; Alloy B with Alloy E.

$$\frac{\dot{\epsilon}_s \text{ (Alloy C)}}{\dot{\epsilon}_s \text{ (Alloy A)}} = \frac{(d^3/\lambda r_v)_C}{(d^3/\lambda r_v)_A} \tag{16a}$$

$$\frac{\dot{\epsilon}_s \text{ (Alloy E)}}{\dot{\epsilon}_s \text{ (Alloy B)}} = \frac{(d^3/\lambda r_v)_E}{(d^3/\lambda r_v)_B} \tag{16b}$$

The calculated creep rate ratios for Equation (16a) and (16b) are 2.6 and 1.5, respectively. These values are in very good agreement with the experimental ratios determined from Figure 15; $\dot{\epsilon}_s$ (Alloy C)/$\dot{\epsilon}_s$ (Alloy A) = 2.4 at 2000 psi to 1.9 at 6000 psi; and $\dot{\epsilon}_s$ (Alloy E)/$\dot{\epsilon}_s$ (Alloy B) = 1.2 over the stress range 4-9,000 psi. This agreement together with the internal stress calculations, the structural studies, and the observation that the experimental activation energy for creep is equal to Q_{sd} in nickel, lends support to the dislocation climb model represented by Equation (14).

CONCLUSIONS

It is concluded that the rate-controlling process for creep of the five experimental Ni-ThO_2 alloys is the climb of edge dislocations over ThO_2 particles. A modified version of the Ansell-Weertman climb theory satisfactorily explains the experimental creep results. In comparing the effects of particle size and spacing on the creep rate, it is important to do so only for alloys with equivalent initial structures, (i. e., for alloys which have approximately the same internal stress levels).

ACKNOWLEDGMENTS

The authors are grateful to Drs. D. J. I. Evans and R. W. Fraser of Sherritt-Gordon Mines Ltd. for kindly donating the experimental Ni-ThO_2 alloys. The assistance of Messrs. G. F. Mead and G. A. Wheeler and Miss Marjorie R. Cantin with the experimental work is also gratefully acknowledged.

REFERENCES

(1) Kelly, A., and Nicholson, R. B., Progress in Materials Science, Vol 10, No. 3, Pergamon Press, Oxford (1963).

(2) Ansell, G. S., "The Mechanism of Dispersion-Strengthening – A Review", paper presented at the Oxide Dispersion Strengthening Conference, Bolton Landing, New York (June 27-29, 1966).

(3) Weertman, J., NRL Rept. 5123 (April 15, 1958).

(4) Ansell, G. S., and Weertman, J., AIME Trans., 215, 838 (1959).

(5) McLean, D., Met. Rev., 7, 487 (1962).

(6) Schoeck, G., Creep and Recovery, Am. Soc. Metals, Cleveland (1957), p 199.

(7) Ansell, G. S., and Lenel, F. V., AIME Trans., 221, 452 (1961).

(8) Wilcox, B. A., and Clauer, A. H., AIME Trans., 236, 570 (1966).

(9) Wilcox, B. A., and Clauer, A. H., AIME Trans., 233, 253 (1965).

(10) Wilcox, B. A., and Clauer, A. H., "High Temperature Creep of Ni-ThO_2 Alloys", paper presented at the Oxide Dispersion Strengthening Conference, Bolton Landing, New York (June 27-29, 1966).

(11) Fullman, R. L., Carreker, R. P., and Fisher, J. C., AIME Trans., 197, 657 (1953).

(12) Fraser, R. W., Meddings, B., Evans, D. J. I., and Mackiw, V. N., paper presented at the 1965 International Powder Metallurgy Conference, New York (June 14-17, 1965).

(13) Endter, F., and Gebauer, H., Optik, 13, 97 (1956).

(14) Amelinckx, S., "The Direct Observation of Dislocations", Solid State Physics, Suppl. 6, Academic Press, New York (1964), p 307.

(15) Smithells, C. J., Metals Reference Book, 3rd ed., Vol 2, Butterworth, Washington, D. C. (1962), p 595.

(16) Weertman, J., and Shahinian, P., AIME Trans., 206, 1223 (1956).

(17) Takahashi, S., Iida, J., and Adachi, M., Trans. Nat. Res. Inst. for Metals (Japan), 6, 231 (1964). See also p 376.

(18) McLean, D., and Hale, K. F., Structural Processes in Creep, The Iron and Steel Inst. (1961), p 19.

(19) Lytton, J. L., Barrett, C. R., and Sherby, O. D., AIME Trans., 233, 1399 (1965).

(20) Ham, R. K., Phil. Mag., 6, 1183 (1961).

(21) Low, J. R., Jr., Progress in Materials Science, Vol 12, No. 1, Pergamon Press, Oxford (1963).

(22) Beachem, C. D., Trans. ASM, 56, 318 (1963).

(23) Ashby, M. F., Z. Metallk., 55, 5 (1964).

(24) McCall, J. L., and Boyd, J. E., Battelle Mem. Inst., research on Contract NAS 3-7611.

(25) Kocks, U. F., Phil. Mag., 13, 541 (1966).

APPENDIX

COMPARISON BETWEEN TRANSMISSION AND REPLICA ELECTRON MICROSCOPY AS TECHNIQUES FOR MEASURING PARTICLE-SIZE DISTRIBUTIONS

APPENDIX

COMPARISON BETWEEN TRANSMISSION AND REPLICA ELECTRON MICROSCOPY AS TECHNIQUES FOR MEASURING PARTICLE-SIZE DISTRIBUTIONS

Although replica electron microscopy (both extraction and direct replication) has been used by various investigators to measure particle sizes, transmission microscopy was preferred for this study on the five experimental Ni-ThO_2 alloys. This choice was made because not only can particle size be measured by transmission microscopy, but dislocation structures can be studied simultaneously.

However, on one alloy (Alloy B), a comparison was made between direct replication and transmission microscopy. In each case about 800 particles were measured in a Zeiss Particle Size Analyzer from transmission and replica micrographs taken at the same magnification on the same electron microscope. The replicas (on electropolished specimens) were prepared by Mr. B. Buzek at NASA Lewis Research Center using the two-stage parlodian/carbon technique with Pt/C shadowing.

The particle size distributions for both techniques are shown in Figure A-1. The transmission microscopy results are the same as those shown in Figure 2. When measuring particles on replica micrographs, extracted particles were not counted. It was assumed the planar particle diameter, $2r_s$, was measured on the replicas, and for convenience in making comparisons the data in Figure A-1 are converted to true particle diamater $2r_v$ (i.e., $2r_v = 2r_s/\sqrt{2/3}$). It is noted that both the average particle diameter and the calculated mean planar center-to-center particle spacing, d, determined by replication, are approximately twice the values determined from transmission micrographs. This discrepancy is more graphically illustrated in Figure A-2 which compares transmission and replica micrographs at the same magnification. Figure A-2(b) shows a replica where some of the ThO_2 particles have been extracted.

The following factors probably contribute to the discrepancy:

(a) In thinning foils for transmission microscopy, probably some of the larger particles (say with $2r_v \gtrsim 900$ Å) are lost from the foil because of preferential etching at the particle/matrix interface. This loss is not very important when determining the average particle diameter since the number of particles with $2r_v \gtrsim 900$ Å is less than ~1 percent of the total number of particles. However, omission of the larger particle becomes somewhat more important when calculating the particle spacing, d, from Equation (4). Here the volume fraction, f_i, of particles in a given size range enters the calculation, and it takes only a few large particles to give large values of f_i.

(b) When measuring small particles on replica micrographs it is difficult to decide whether the measured diameter is the planar diameter, $2r_s$, or the true diameter, $2r_v$. This arises because the electropolishing and/or etching procedures used for specimen surface preparation can undercut the smaller particles. Thus the measured diameters of fine particles may be $2r_v$ whereas those of the larger particles may be $2r_s$. When averaging the particle size, a value is obtained somewhere between $2r_v$ (avg) and $2r_s$ (avg). However, the

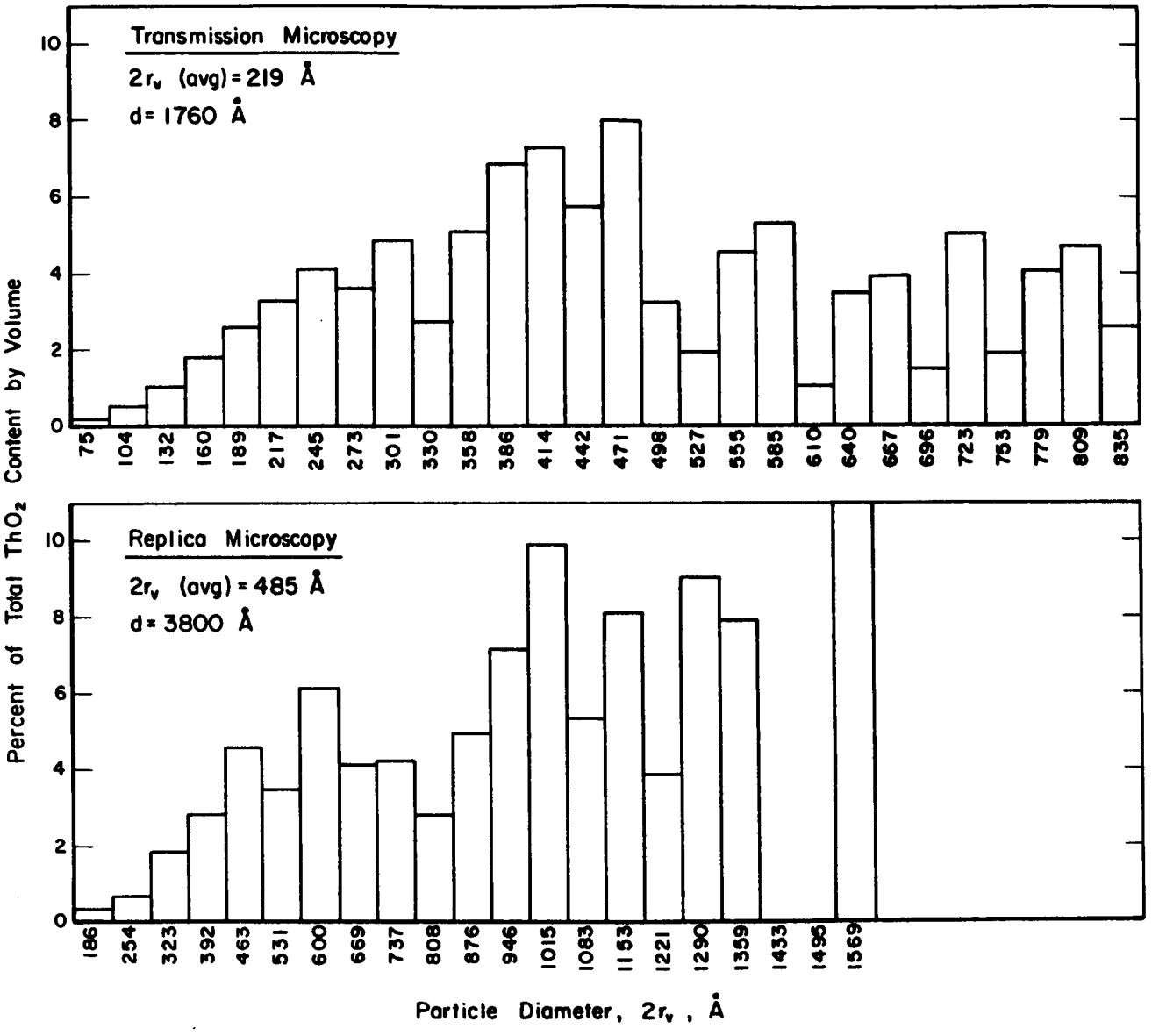

FIGURE A-1. COMPARISON BETWEEN TRANSMISSION AND REPLICA MICROSCOPY AS TECHNIQUES FOR MEASURING PARTICLE-SIZE DISTRIBUTIONS ON ALLOY B

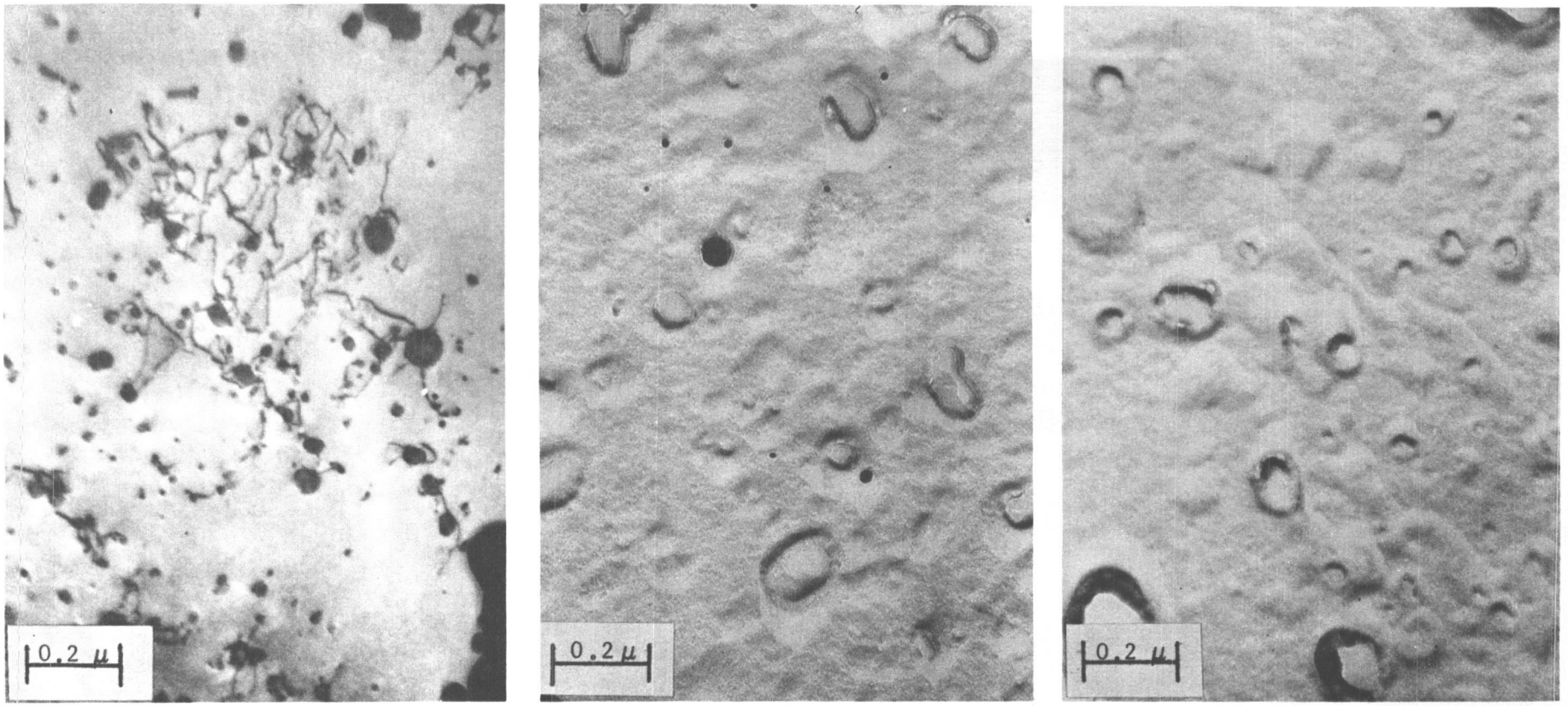

L239 U165 U159

a. Transmission Micrograph

b. Replica Micrograph With Some ThO_2 Particles Extracted

c. Replica Micrograph With No ThO_2 Particles Extracted

FIGURE A-2. COMPARISON OF TRANSMISSION AND REPLICA ELECTRON MICROSCOPY AS A MEANS OF VIEWING ThO_2 PARTICLES, AS-RECEIVED ALLOY B

errors involved here cannot explain the discrepancy observed for Alloy B. For example, if it is assumed that all the particle diameters measured on the replica micrographs are the true diameters ($2r_v$), then the average diameter (Figure A-1) would only decrease from 485 Å to 395 Å, which is still considerably larger than the value of $2r_v$ = 219 Å measured by transmission microscopy.

(c) It is felt that the chief reason for the difference between direct replica and transmission techniques arises from the inherent inaccuracies of the replica method in measuring the smaller particles (those with $2r_v \lesssim$ 150-200 Å). The lack of definition and resolution is illustrated in Figure A-2(b). Here very fine extracted ThO_2 particles are well defined on the replica background. However it is very difficult to accurately measure the finest replicated particles because of the poor definition, and it is occasionally impossible to distinguish between particles and surface asperities or artifacts. It is also very possible that some of the finest particles ($2r_v \lesssim$ 100 Å) are missed by the replication method. These problems lead to large errors when replicas are made of alloys such as Alloy B, where ~60 percent of the particles have diameters <200 Å.

Thus it is concluded that direct replication of dispersion-strengthened metals can lead to sizable errors in particle-size measurements if a large percentage of the particles have diameters $\lesssim$ 150-200 Å. Recent work at Battelle by McCall and Boyd[24] lends support to this conclusion. They have examined fine ThO_2 dispersions in a complex Co-base alloy (1.5-6 vol % ThO_2, with average ThO_2 particle diameters of ~200 Å). Comparisons were made between direct replication and two other techniques: (a) extraction replica and (b) total extraction by dissolution of the matrix. Particle-size distributions determined by the latter two methods gave nearly identical results. However the average particle size determined by direct replication was about twice that given by either of the extraction methods. McCall and Boyd also concluded that direct replication can lead to significant errors in particle-size distributions if a large fraction of the particles have diameters less than ~200 Å.

DISTRIBUTION LIST
CONTRACT NAS3-7615

	Address		No. of Copies
1.	NASA Scientific & Technical Information Facility P. O. Box 33 College Park, Maryland 20740 Attn: NASA Representative RQT-2448		6
2.	NASA Headquarters Washington, D. C. 20546		
	Attn: N. F. Rekos (RAP)		1
	G. C. Deutsch (RRM)		1
	R. H. Raring (RRM)		1
3.	NASA-Lewis Research Center 21000 Brookpark Road Cleveland, Ohio 44135		
	Attn: Report Control Office	M. S. 5-5	1
	Library	M. S. 60-3	2
	G. M. Ault	M. S. 105-1	1
	Technology Utilization Office	M. S. 3-19	1
	Patent Counsel	M. S. 501-3	1
	I. I. Pinkel	M. S. 5-3	1
	Paul Hacker	M. S. 5-3	1
	J. Howard Childs	M. S. 60-4	1
	F. H. Harf	M. S. 60-6	5
	A. E. Anglin	M. S. 60-6	1
	Dr. W. H. Roudebush	M. S. 60-6	1
	John H. DeFord	M. S. 60-5	1
	J. W. Weeton	M. S. 49-1	1
	Dr. W. S. Cremens	M. S. 49-1	1
4.	FAA Headquarters 800 Independence Avenue, S. W. Washington, D. C. 20553		
	Attn: Brig. Gen. J. C. Maxwell		1
	F. B. Howard SS/120		1
5.	U. S. Atomic Energy Commission Washington, D. C. 20545		
	Attn: Jules Simmons		1
	Technical Reports Library		1

DISTRIBUTION LIST
(Continued)

	Address	No. of Copies
6.	Oak Ridge National Laboratory Oak Ridge, Tennessee 37830 Attn: M. L. Picklesimer	1
7.	Air Force Office of Scientific Research Propulsion Research Div. USAF Washington, D. C. 20525 Attn: Dr. M. Slawsky	1
8.	NASA-Goddard Space Flight Center Greenbelt, Maryland 20771 Attn: Dr. H. Fracnkel	1
9.	Defense Documentation Center (DDC) Cameron Station 5010 Duke Street Alexandria, Virginia 22314	1
10.	Headquarters Wright Patterson AFB, Ohio 45433 Attn: MAMP: C. Lombard	1
	MATB: Lt. A. Lopez	1
	MAAM: Technical Library	1
	AFSC-FTDS: Sm. Sgt. J. C. Ingram, Jr.	1
	AFML: Dr. A. M. Lovelace	1
	MAM: Dr. H. M. Burte	1
	MAMP: I. Perlmutter	1
	SESOS: J. L. Wilkins	1
11.	Department of the Navy ONR, Code 429 Washington, D. C. 20525 Attn: Dr. R. Roberts	1
12.	U. S. Army Aviation Materials Lab. Fort Eustis, Virginia 23604 Attn: John White, Chief, SMOFE-APG	1
13.	Chief, Bureau of Naval Weapons Dept. of the Navy Washington, D. C. 20525 Attn: T. F. Kearns	1
	RRMA: Nathan E. Promisel	1

DISTRIBUTION LIST
(Continued)

	Address	No. of Copies
14.	NASA-Langley Research Center Langley Field, Virginia 23365 Attn: Library Richard Pride	 1 1
15.	NASA-Marshall Space Flight Center Huntsville, Alabama 35812 Attn: Library	 1
16.	Jet Propulsion Laboratory 4800 Oak Grove Drive Pasadena, California 91103 Attn: Library	 1
17.	Army Materials Research Agency Watertown Arsenal Watertown, Massachusetts 02172 Attn: S. V. Arnold, Director	 1
18.	NASA-Ames Research Center Moffet Field, California 94035 Attn: Library	 1
19.	NASA-Goddard Space Flight Center Greenbelt, Maryland 20771 Attn: Library	 1
20.	NASA-Manned Space Flight Center Houston, Texas 77058 Attn: Library Norman Chaffee	 1 1
21.	NASA-Flight Research Center P. O. Box 273 Edwards, California 93523 Attn: Library	 1
22.	NASA Western Operations 150 Pico Blvd. Santa Monica, California 90406 Attn: Library	 1
23.	Department of the Navy U. S. Navy Marine Engineering Lab. Annapolis, Maryland Attn: Dr. Klaus M. Zwilsky	 1

DISTRIBUTION LIST
(Continued)

	Address	No. of Copies
24.	Air Reduction Co. Central Research Lab. Murray Hill, New Jersey Attn: Dr. E. Gregory	1
25.	American Society for Metals Metals Park Novelty, Ohio Attn: Dr. Taylor Lyman	1
26.	SST Unit Chief Boeing Company P. O. Box 733 Renton, Washington 98055 Attn: Walter E. Binz, Jr.	1
27.	AiResearch Manufacturing Company 9851-9951 Sepulveda Blvd. Los Angeles, California 90009 Attn: Harold H. Block, Senior Metallurgist	1
28.	Pratt & Whitney Aircraft East Hartford, Connecticut 06108 Attn: Elihu F. Bradley Chief, Materials Engineering	1
29.	Lockheed Missile and Space Co. Palo Alto, California 94304 Attn: Dr. E. C. Burke, Materials Science Lab. Dr. T. E. Tietz, Materials Science Lab.	1 1
30.	Ohio State University Columbus, Ohio 43210 Attn: Prof. M. G. Fontana, Chairman Department of Metallurgical Engineering	1
31.	University of California at Los Angeles Los Angeles, California Attn: Dr. George Hoffman	1
32.	Solar/2200 Pacific Highway San Diego, California 92112 Attn: John V. Long, Director of Research	1
33.	Titanium Metals Corp. of America 233 Broadway New York, New York 10007 Attn: Ward Minkler, Mgr. of Technical Service	1

DISTRIBUTION LIST
(Continued)

	Address	No. of Copies
34.	Narmco Research & Development Div. Whittaker Corp. 3540 Aero Court San Diego, California 92123 Attn: Dr. Frank J. Riel, Technical Director	1
35.	Gordon McKay Laboratory Harvard University Cambridge, Massachusetts 02138 Attn: Dr. M. F. Ashby	1
36.	Advanced Materials Research & Development Lab. Pratt & Whitney Aircraft North Haven, Connecticut 06473 Attn: Dr. D. H. Boone	1
37.	Solid State Sciences Div. The Franklin Institute Philadelphia, Pennsylvania 19103 Attn: Dr. H. Conrad	1
38.	Metals and Ceramics Div. Air Force Materials Lab. Wright-Patterson Air Force Base, Ohio 45433 Attn: T. D. Cooper	1
39.	University of California Hearst Mining Bldg. – Room 268 Berkeley, California 94720 Attn: Prof. J. E. Dorn Dr. T. Langdon	1 1
40.	Materials Division Central Electricity Research Laboratory Kingston Road Leatherhead, Surrey England Attn: Dr. R. K. Ham	1
41.	Dept. of Materials Science Pennsylvania State University University Park, Pennsylvania 16802 Attn: Prof. M. C. Inman	1

DISTRIBUTION LIST
(Continued)

	Address	No. of Copies
42.	Ford Scientific Lab. 20,000 Rotunda Drive Dearborn, Michigan 48124 Attn: Dr. T. L. Johnston Dr. C. Laird	 1 1
43.	Central Electricity Generating Board Berkeley Nuclear Lab. Berkeley, Gloucestershire England Attn: Dr. R. B. Jones	 1
44.	Dept. of Materials Science Stanford University Stanford, California 94305 Attn: Prof. O. D. Sherby Prof. C. Barrett	 1 1
45.	Materials & Processes Lab. General Electric Co. Schenectady, New York 12301 Attn: C. T. Sims	 1
46.	Department of Metallurgy Pembroke Street Cambridge University Cambridge England Attn: G. C. Smith	 1
47.	Curtiss-Wright Corp. Metals Processing Div. Buffalo, New York 14215 Attn: B. Triffleman	 1
48.	Aerospace Corp. El Segundo, California 90245 Attn: Dr. J. E. White Dr. K. Kamber	 1 1
49.	Defense Metals Information Center (DMIC) Battelle Memorial Institute 505 King Avenue Columbus, Ohio 43201	 1
50.	E. I. DuPont de Nemours & Co. Metal Products Sales Wilmington, Delaware 19898 Attn: Dr. W. I. Pollock	 1

DISTRIBUTION LIST
(Continued)

	Address	No. of Copies
51.	General Electric Company Advanced Technology Lab. Schenectady, New York 12305	1
52.	General Electric Company Materials Devel. Lab. Oper. Advanced Engine & Tech. Dept. Cincinnati, Ohio 45215 Attn: L. P. Jahnke	1
53.	General Motors Corp. Allison Div. Indianapolis, Indiana 46206 Attn: D. K. Hanink, Materials Lab.	1
54.	Ilikon Corp. Natick Industrial Center Natick, Massachusetts Attn: Dr. L. J. Bonis	1
55.	International Nickel Co. 67 Wall Street New York, New York 10005 Attn: R. R. Dewitt	1
56.	International Nickel Co. Huntington, W. Virginia Attn: Library	1
57.	International Nickel Co. P. D. Merica Research Lab. Sterling Forest Suffern, New York 10901 Attn: Dr. F. Decker Dr. H. Merrick	1 1
58.	Arthur D. Little, Inc. 20 Acorn Park Cambridge, Massachusetts Attn: Dr. B. Bovarnick	1
59.	Lockheed Palo Alto Research Labs. Materials & Science Lab 52-30 3251 Hanover Street Palo Alto, California Attn: Dr. Clause G. Goetzel	1

DISTRIBUTION LIST
(Continued)

	Address	No. of Copies
60.	Massachusetts Institute of Technology Metallurgy Dept. Cambridge, Massachusetts Attn: Prof. N. J. Grant	1
61.	Melpar, Inc. 3000 Arlington Blvd. Falls Church, Virginia Attn: N. Fushillo	1
62.	National Research Corp. 70 Memorial Drive Cambridge, Massachusetts 02142 Attn: Technical Information Center	1
63.	New England Materials Lab., Inc. Medford, Massachusetts Attn: Dr. R. Widmer	1
64.	Rensselaer Poly Tech. Troy, New York Attn: Prof. Fritz V. Lenel Prof. George S. Ansell	1 1
65.	Sherritt Gordon Mines, Ltd. Research & Development Div. Fort Saskatchewan Alberta, Canada Attn: Dr. R. W. Frazer Dr. J. I. Evans	1 1
66.	Sylvania Electric Products, Inc. Chemical & Metallurgical Div. Towanda, Pennsylvania Attn: Dr. J. S. Smith	1
67.	TRW Electromechanical Div. TRW Inc. 23555 Euclid Avenue Cleveland, Ohio 44117 Attn: G. Doble	1
68.	Universal-Cyclops Steel Corp. Bridgeville, Pennsylvania Attn: C. P. Mueller	1

DISTRIBUTION LIST
(Continued)

	Address	No. of Copies
69.	Vitro Corp. Vitro Laboratories 200 Pleasant Valley Way West Orange, New Jersey Attn: Dr. S. Grand	1
70.	United Aircraft Corp. 400 Main St. East Hartford, Connecticut 06108 Attn: Research Div. Library	1
71.	Northwestern University Dept. of Metallurgy Evanston, Illinois Attn: Prof. J. Weertman	1
72.	Cast Institute of Technology University Circle Cleveland, Ohio 44106 Attn: Prof. L. Leonard Dept. of Metallurgy	1